CHARACTERIZATION OF CAKING AND CAKE STRENGTH IN A POTASH BED

A Thesis

Submitted to the College of Graduate Studies and Research

in Partial Fulfillment of the Requirements for the Degree of

Master of Science

In the Department of Mechanical Engineering

University of Saskatchewan

By

Yan WANG

Saskatoon, Saskatchewan

PERMISSION TO USE

The author grants permission to the University of Saskatchewan Libraries to make this thesis available for inspection. Copying of this thesis, in whole or in part, for scholarly purposes may be granted by my supervisors (Prof. Robert W. Besant and Prof. Richard W. Evitts), the head of the Department of Mechanical Engineering, or the Dean of the College of Engineering. It is understood that any copying or publication or use of this thesis or parts thereof for financial gain shall not be allowed without my written permission. It is also understood that due recognition to me and the University of Saskatchewan must be granted in any scholarly use which may be made of any material in this thesis.

Requests for permission to copy or to make other use of the material in this thesis in whole or in part should be addressed to:

Head, Department of Mechanical Engineering
University of Saskatchewan
57 Campus Drive
Saskatoon, SK
Canada S7N 5A9

ABSTRACT

When a water soluble granular fertilizer, such as potash, is wetted and then dried during storage and transportation processes, clumps or cakes often form in the material even when the maximum moisture content is less than 1% by mass. In order to avoid or decrease these occurred cakes, it is essential to characterize cake strength and to explore the process of cake formulation or caking through theoretical/numerical analysis. In this thesis, both experimental measurements of cake strength and theoretical/numerical simulations for recrystallization near a contact point are used to investigate the relationship between the caking process and the cake strength for important factors such as initial moisture content and drying time.

In this research, a centrifugal loading method has been developed to determine cake strength in a caked ring specimen of potash fertilizer where internal tensile stresses dominate. Research on fracture mechanics states that brittle materials, such as caked potash, fail at randomly positioned fracture surfaces in tension – so the centrifuge test method is well suited to provide good data. A two-dimensional plane stress analysis was used to determine the area-averaged tensile stress at the speed of the centrifuge when each specimen fractures. Repeated tests and uncertainty calculations give data with a narrow range of uncertainty.

The centrifuge test facility was used for a series of tests in which the initial moisture content, drying time, particle size and chemical composition (i.e. magnesium content) of the samples were varied. For particle sizes in the range from 0.85 to 3.35

mm, experimental data show that the cake strength increased linearly with initial moisture content for each drying method and particle size, and decreased with increasing particle size for each initial moisture content and drying method. As well, it was also found that cake strength will increase essentially linearly with magnesium content from 0.02% to 0.1% for samples with the same initial moisture content, particle size and drying method. All data show that potash samples tend to form a stronger cake with a slower drying process.

A theoretical/numerical model is presented in this thesis to simulate ion diffusion and crystallization near one contact point between two potash (KCl) particles during a typical drying process. The effects of three independent factors are investigated: initial moisture content; evaporation rate; and degree of supersaturation on the surface surrounding the contact point. The numerical results show that the mass of crystal deposition near the contact point will increase with increased initial moisture content and decreased evaporation rate. These numerical predictions for recrystallization near the contact point are consistent with the experimental data for the cake strength of test samples of particle beds. With variations in the solid crystal surface degree of supersaturation near the contact point, simulations showed up to 5 times the increase in the crystal mass deposition near the contact point. This prediction of increased roughness is consistent with another experimental investigation which showed that the surface roughness of NaCl and KCl surfaces increased by a factor of five after one wetting and drying process.

ACKNOWLEDGMENTS

I would like to firstly express my sincere and deepest appreciation to my supervisors, Professor Robert W. Besant and Professor Richard W. Evitts. You showed me different ways to approach a research problem and the need to be persistent to accomplish any goal. Without your expertise, encouragement, patience and guidance throughout this work, I would not have completed my Master's program.

The grateful thanks are also extended to my advisory committee members: Professor Allan Dolovich who provided a lot of advice and impetus for the portion of applied mechanics in this project and Professor Carey J. Simonson for your valuable comments and suggestion.

Sincere thanks to Dan Gillies who collected most of the data presented in Chapter 3. Thanks also to Mr. Dave Deutscher, Mr. Chris James, Mr. Hans-Jürgen Steinmetz, and Mr. Dave G. Crone for your help with the experimental studies.

Heartfelt thanks to my families: my parents and father-in-law for your encouragement during my period of studies. Special thanks are given to my wife for your everlasting love and support.

Financial assistance from the Natural Science and Engineering Research Council of Canada (NSERC) and the Potash Corporation of Saskatchewan (PCS) is also acknowledged and appreciated.

DEDICATION

This thesis is dedicated to my wife, Yuwei Li

TABLE OF CONTENTS

LIST OF TABLES

LIST OF FIGURES

NOMENCLATURE

ENGLISH SYMBOLS

A surface area of crystal growth, [m^2]

B coefficient

c electrolyte concentration, [mole/m^3]

C dimensionless concentration

C_1 defined coefficient

C_1' defined coefficient

C_2 defined coefficient

C_2' defined coefficient

C_a dimensionless concentration on solid surface of particle for $0 \le R \le 1, Z = 0$

C_b dimensionless concentration on solid surface of particle for $R > 1, Z = 0$

c_s solubility, [mole/m^3] or [g/100g water]

D diameter of sample [mm], or diffusion coefficient of an electrolyte in water, [m^2/s]

D_+ diffusion coefficient for a cation, [m^2/s]

D_- diffusion coefficient for an anion, [m^2/s]

d_o average distance between contact points on one particle, [mm]

d_p particle diameter [mm]

d_{pm} mean particle diameter [mm]

E Young's modulus [Pa]

E_b measured Young's modulus for caked potash sample [Pa]

h height of potash bed [mm]

H_R Dimensionless height of deposited crystal layer on potash particle surface

k k^{th} measurement

L height of cylindrical potash sample [mm]

M_c dimensionless crystal mass deposition inside the contact region $0 \le R \le 1, Z = 0$

m_c mass of crystal deposition inside contact region $0 \le R \le 1, Z = 0$, [mole]

m_{ci} initial mass of KCl in the liquid film solution inside the contact region [mole]

M_g magnesium content [%]

N number of test samples, or dimensionless crystal mass deposition per unit area

n_c average mass of crystal deposition per unit area inside the contact region, [mole]

N_c dimensionless crystal mass deposition per unit area inside the contact region

n_i initial mass of KCl salt per unit area in the thin film solution [mole]

N_o dimensionless crystal mass deposition per unit area at $r = r_o$

n_o mass of crystal deposition per unit area at $r = r_o$ [mole]

$\bar{q}$ mass of crystal growth on a surface, [mole]

r radial position [m], or space variable for the cylindrical coordinate

r radius of cylindrical shell [m]

R dimensionless space variable, r/r_c

r_c thickness of contact region, [m]

r_m mean radius of cylindrical shell [m]

R_o dimensionless outer radius of cylinder

s position of moving evaporation surface, [m]

S dimensionless position of moving evaporation surface, or estimate of the standard deviation of sample mean

S^* relative moving boundary position, S/δ

S_o dimensionless position of moving evaporation surface before drying, δ/r_c

S_m specific surface area per unit mass for potash bed, [m^2/kg]

t time [s], or student multiplier

t_c time constant [min]

T temperature [^oC]

u displacement [m]

U uncertainty of measurement

u_s constant moving boundary velocity, [m/s]

U_S dimensionless moving boundary velocity

v_s volume of infinitesimal evaporation layer, [m^3]

V air velocity through the specimen [m/s]

V_s dimensionless volume of infinitesimal evaporation layer

x the length of the diffusion path, [m]

X initial moisture content, [w/w %]

X_b potash bed moisture content, [w/w %]

z axial position [m], or space variable in cylindrical coordinate

Z dimensionless space variable

z_- charge number for anion

z_+ charge number for cation

GREEK SYMBOLS

δ thickness of thin film before the start of the drying process, [m]

ΔD displacement in lateral direction [mm]

ΔL displacement in uniaxial direction [mm]

ΔZ dimensionless space step in Z direction

Δt drying period [h], or time step [s]

ε porosity for potash bed, or tolerance

ε_l strain in lateral direction

ε_a strain in uniaxial direction

θ angular position (radians)

v Poisson's ratio

ξ dimensionless tensile stress $\sigma/(\rho\omega^2 r_m^{\ 2})$

ξ_c dimensionless radial stress at inner surface (i.e. at $\psi = \psi_i$)

ρ bulk density of a potash bed [kg/m^3]

ρ_w density of water [kg/m^3]

σ stress [Pa]

σ_c loading stress [Pa]

τ dimensionless time(i.e. Fourier number for mass transfer), or shear stress [Pa]

Φ relative humidity [%]

ψ dimensionless radius of cylindrical shell r / r_m

ω angular speed (rad/s)

SUBSCRIPTS

i inner side

o outer side

r radial

θ circumferential

CHAPTER 1

INTRODUCTION

1.1 General

As the most important potassium fertilizer, potash is widely used around world. The final potash product is primarily comprised of sylvite (i.e. potassium chloride (KCl)), but it contains internal and surface impurities. The mineral, sylvite, is mined from naturally occurring ore bodies deposited about 1 km underground. After KCl is produced and processed in a solution or flotation process, the final products are sold as different types, each with a different particle size distribution. Standard and granular potash are the two main commercial products for which the particle sizes range from 0.2 to 2 mm for the standard and 2 mm to 4 mm for the granular products. Figure 1-1 shows these two kinds of potash produced by Saskatchewan Potash Corporation, Canada. Potash can appear as white crystals produced by a solution mining process or red crystals with traces of iron oxide produced by a mining machine and processed by a floatation process. Almost all potash fertilizers are handled as bulk granular products. Figure 1-2 shows the photography of a few potash particles with enlarged images for particle size ranges of (a) 0.85 mm ~1.18 mm and (b) 2.85 mm~3.30 mm.

(a) (b)

Figure 1-1: Two types of potash sold as commercial products (a) Standard Potash and (b) Granular Potash

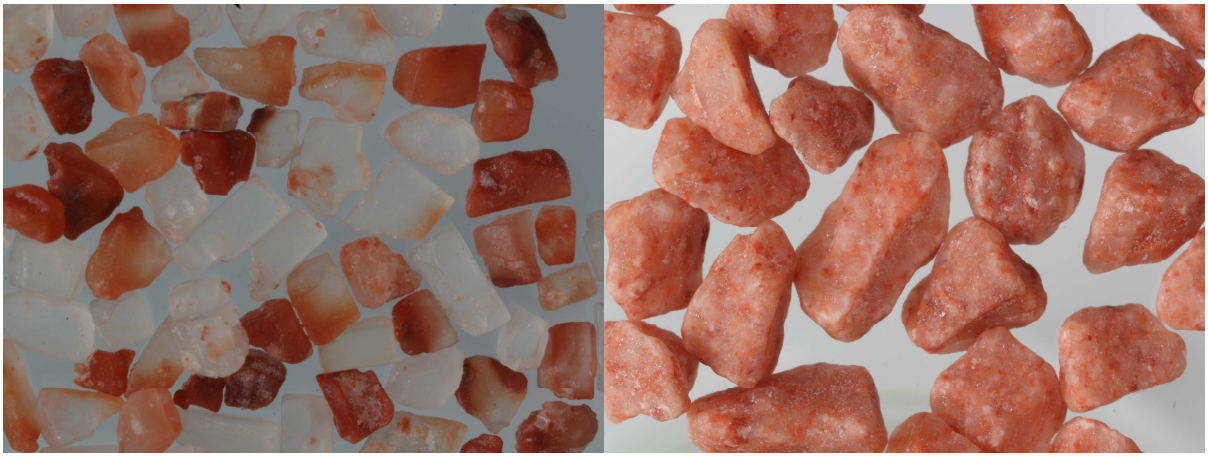

(a) (b)

Figure 1-2: Photos of a few potash particles with enlarged images for particle size ranges (a) from 0.85 mm to 1.18 mm and (b) from 2.85 mm to 3.30 mm

Figure 1-3 also shows a photo of a single potash particle with a mean particle diameter of about 3 mm. Both Figure 1-2 and 1-3 show that each potash particle has an irregular shape with sharp crystalline edges and the shape of each particle is unique.

Figure 1-3: Enlarged image of a single potash particle ($d_{pm} \approx 3.00$ mm)

After mining and processing, potash particles may trap some sodium chloride and magnesium chloride crystals within or on the surface of the particles such as halite (NaCl) and carnallite ($KMgCl_3 \cdot 6H_2O$) microcrystals. The floatation or recrystallization process, followed by a subsequent dying process to remove impurities in potash, results in the surfaces of potash particles coated by a thin layer of mixed crystals which are composed of small amounts of NaCl (halite) and $KMgCl_3 \cdot 6H_2O$ (carnallite) with some local compositional variations.

When exposed in humid air, a potash particle will adsorb moisture from the surrounding air during storage and transportation. Subsequently, when the relative humidity drops, moisture will be removed from the granular particles by a drying

process. If this occurs at moisture contents greater than about 0.2%, big chunks or clumps may form in potash beds. This process is called caking. Figure 1-4 shows the caked potash samples. Experience and past research has revealed that the prime handling problem with bulk fertilizer products such as potash is caking. Clumps or chunks in potash impede the handling and flow of granular materials and are especially unfavorable for the uniform distribution of potash particles in the soil by most agricultural machines.

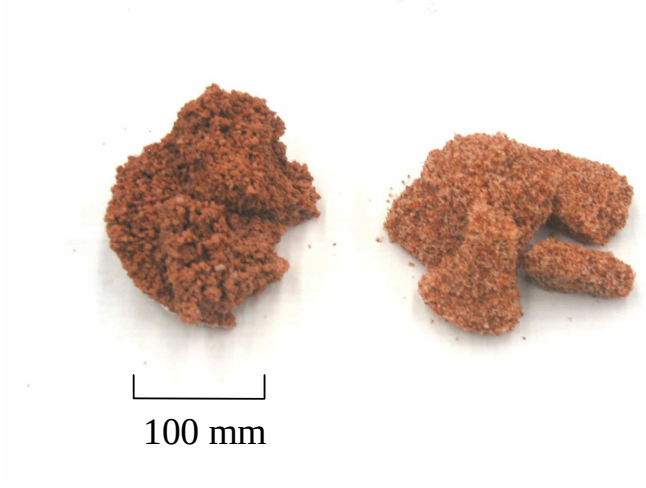

Figure 1-4: Caked standard and granular potash samples

Every year, millions of tons of potash fertilizer products are exported to the United States, Brazil, China, Australia and other overseas markets. Before potash is eventually spread in the soil, it is usually stored in warehouses or sheds that have no temperature and humidity control. During storage and transportation, potash may experience large temperature and humidity changes. Moisture accumulation on potash surfaces will penetrate toward the inside of a potash bed over time. For this reason, significant quantities of potash are wasted due to caking. Therefore, understanding the

caking process and caking physical-chemical mechanism is essential to devise practical means of preventing or reducing caking. In this research, a direct measurement of cake strength subject to a range of test conditions is performed using a newly designed test facility so that the cake strength of a bed of potash can be accurately quantified. To understand the measured data, a theoretical/numerical model of the caking process is needed so as to quantify the physical-chemical mechanism.

1.2 Caking in Potash

The caking process in bulk potash products is a complex chemical and physical process which involves coupled heat and moisture transfer in potash beds. The caking sequence always starts with moisture accumulation which causes dissolution, and ends with a dying process (i.e. a water evaporation process) which results in recrystallization from the aqueous solution films on particle surfaces.

For an aqueous chemical solution system consisting of ions of K, Na, Mg, and Cl from molecules of KCl-NaCl-$MgCl_2$-H_2O, the corresponding room temperature equilibrium solid phase products (precipitation products) are sylvite, halite and carnallite, if there are sufficient potassium ions in the solution. These salts are hygroscopic with deliquescent relative humidities of about 52% for carnallite, 75% for halite, and 85% for sylvite. The existence of these surface impurities causes the potash-moisture interactions to significantly deviate from that of pure potassium chloride. A relative humidity of 52% is the critical relative humidity for the onset of water vapor adsorption and condensation on potash when carnallite is present on particle surfaces. When a dry potash sample is exposed to ambient air relative humidity above 52%, the

potash will absorb water vapor which forms an aqueous salt solution layer on the particle surfaces. The dissolution process of different salts will increase with increasing relative humidity and there will be interactions among the three types of dissolved salts such that, above 52% relative humidity, the surface carnallite will tend to dissolve completely, above 75% the halite will dissolve and above 85% the sylvite will dissolve (Peng et al., 1999).

Moisture adsorbed into potash beds and accumulated on the surface of any exposed particles will dissolve the solid potash to from a thin layer or film of electrolytic solution on the surface of each particle. When this potash is dried, the aqueous solution layer will evaporate and KCl will recrystallize on the particle surfaces. Previous research showed that the caking process of potash is mainly caused by the growth of crystal bridges at or near contact points between particles as shown in Figure 1-5 (Kollmann and Tomas 2001). When crystal bridges are distributed extensively on many adjacent particles in a bed, the dried bed is caked. These crystal bridges develop during storage and transportation due to continuous internal water interactions and thermal effects which result in the deposition of crystals under certain conditions from the salt solutions present in potash bed. There are many factors that influence the rate and extent of potash caking. Chen (2004) reviewed such factors including chemical composition and hygroscopicity, particle size and packing, moisture content, relative humidity of adjacent air, pressure in potash pile and temperature.

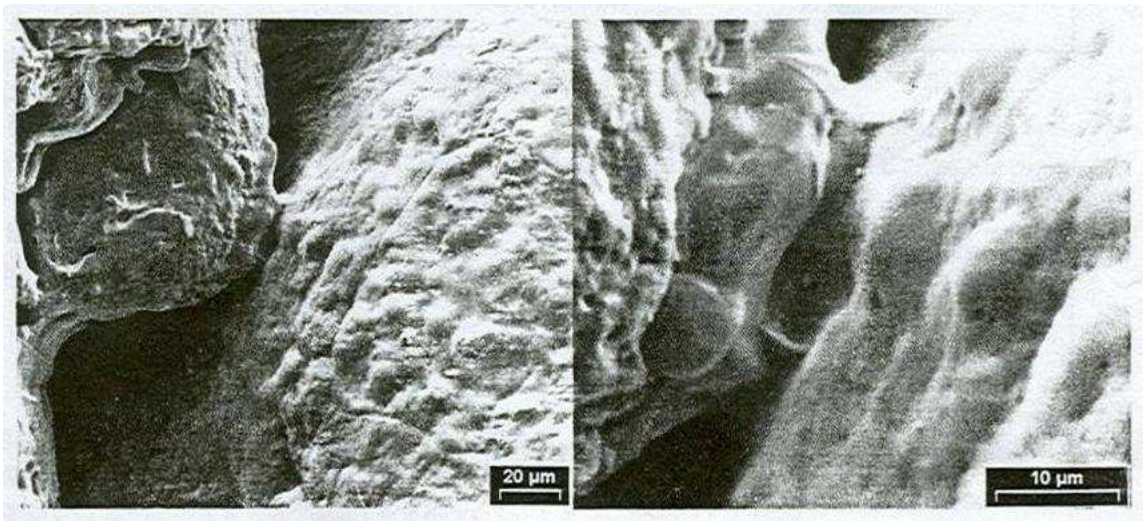

Figure 1-5: SEM image of a solid bridge between two particles of potash due to a recrystallization microprocess (Kollmann and Tomas 2001)

In this study, it is expected that the formation of cakes or the recrystallization of salts near or at the contact points between particles depends on the initial moisture content, the rate of drying and chemical composition of the salt solution on the surfaces of the particles. Accurate measurements of cake strength are needed for each of these important factors. A theoretical/numerical model is needed to simulate the recrystallization process near or at contact points between particles during drying processes.

Studying the heat and moisture transfer in potash beds and understanding the mechanism of caking has been the subject of several research studies in recent years and is of considerable engineering interest because of its economic impact. Many papers have been published in a variety of journals concerning the storage handling, and caking of bulk materials such as potash.

1.3 Literature review of potash products

The previous research works concerning caking of bulk materials are reviewed in different areas. Some investigations on heat and moisture transfer in potash at the University of Saskatchewan are reviewed in section 1.3.1, cake strength studies for bulk materials in section 1.3.2, cake strength measurement in section 1.3.3, and studies on recrystallization processes in section 1.3.4.

1.3.1 University investigations of heat and moisture transfer

In recent years, several research investigations on heat and moisture transfer in potash have been performed at the University of Saskatchewan. Peng et al. (1999) modelled the thermodynamic state of potash over a range of relative humidities and predicted the moisture content (i.e. as an aqueous solution of three different salts, KCl, NaCl and $KMgCl_3 \cdot 6H_2O$, each with a unique concentration). A solubility analysis of potash fertilizer at thermodynamic equilibrium was presented. The equilibrium constant method was used to analyze and solve the equilibrium dissolution reaction of potash with moisture as a function of the adjacent air relative humidity or surface solution activity. A critical relative humidity for the existence of a surface aqueous solution saturated with three solid salts (sylvite, halite and carnallite) but predominately carnallite was found around 52% relative humidity with slight temperature dependence. This relative humidity is defined as the critical relative humidity for the onset of condensation on potash when a small fraction of carnallite exists on the particle surfaces. When the environmental relative humidity is lower than 52%, the potash will adsorb a small

amount of water vapour and several layers of adsorbed water may exist on the surface. When the relative humidity exceeds 52%, water vapour will condense and cause dissolution of the potash salts until a new equilibrium is reached. The relationship between the relative humidity and the equilibrium moisture content was established by the dissolution calculation using the Pitzer chemical equilibrium model for multi-species electrolyte.

Peng et al. (2000) studied the heat and mass transfer due to air flow through a granular potash bed experimentally and numerically. They used an experimental setup to measure the temperature and air humidity response and mass gain of a potash bed subject to a step change in air flow down through the bed. The transient temperature and moisture content distribution was predicted using a porous medium mathematical/numerical model. Experimental and numerical results showed that non-equilibrium internal moisture and heat transfer processes existed in the bed with significant differences between the pore air properties and particle temperature and surface relative humidity. The dissolution of potash, due to humid air flow through a potash bed, causes a significant temperature rise and humidity decrease in the exhaust air. The adsorption and dissolution during potash-water vapour interaction causes the temperature of solid particles to be significantly higher than the air temperature, necessitating the use of two coupled energy equations, one for the gaseous component and the other for the solid-liquid component of the bed.

Zhou (2000) measured the macroscopic properties of each of six different types of potash products and measured the moisture accumulation in a test bed of two potash fertilizer products, standard and granular. He developed a one-dimensional transient

numerical model to simulate coupled heat and moisture diffusion in a test bed, including adsorption/dissolution and condensation at the air-potash interface. Experimental data were compared to the numerical simulations for a range of operating conditions.

Arinze et al. (2000) collected and correlated experimental data for thin-layers during moisture adsorption, drying and caking for different potash products. Analysis of these data showed the caking propensity of potash products was strongly dependent on the surrounding air humidity and storage time. Empirical correlations were developed to predict moisture uptake, drying time and potential for caking in laboratory potash test samples. Arinze et al. (2001) studied the factors that favour caking in potash and suggested an empirical relationship between potash cake strength as determined qualitatively and peak moisture content, storage time and self-imposed pressure. Other factors that were not investigated but may influence the extent of a potash cake include: chemical composition on the particle surfaces; particle size, shape and packing; the history of ambient air humidity adjacent to the test bed; hydrostatic pressure in the test bed; and atmospheric temperature and pressure variations.

Peng et al. (2001) measured the enthalpy change or the thermal energy release during a potash-moisture interaction using a method developed by Tao et al. (1992) for two typical granular potash fertilizers with slightly different surface chemical composition. It was found that the combined enthalpy change, including heat of adsorption, condensation and dissolution is a function of the moisture content and trace chemical impurities on potash particles surface. At low moisture content, the enthalpy change is much larger than the combined heat of dissolution and latent heat of evaporation/condensation, which declines with moisture content so that for moisture

contents above 1% the latent heat effects equal that for water in contact with a salt mixture.

A dry air wall jet was studied by Gao (2001) which may be used to protect potash from humid air in large storage buildings. The wall jet mean velocity, relative humidity and moisture accumulation were investigated using an experimental test facility for measuring changes in the wall jet. The decay of maximum velocity, growth of the jet half-width, and self-similarity of the wall jet variation with distance from the jet exit were determined from measured data. The skin friction coefficient and mass transfer coefficient were calculated for the fully developed flow region of the wall jet. Studying fully developed wall jet air flow over both rough and smooth surfaces showed that the maximum velocity decays much more rapidly for rough surfaces than for smooth surfaces and that wall jet separation can readily occur due to the heating effects of water vapour condensation when the supply air relative humidity is above 60%.

Chen et al. (2004) experimentally and theoretically investigated the important properties required to determine moisture transfer by capillarity, gravity, and diffusion within a particle bed of potash such as porosity, permeability, specific surface area, and irreducible saturation for narrow ranges of particle size. Porosity and permeability were directly measured and specific surface area was calculated using the Carman correlation. The irreducible saturation level in a granular potash bed was deduced from experimental data when there was agreement with a theoretical/numerical simulation of moisture movement by capillarity and gravity. It was shown that, for a bed mixture with a wide range of particle sizes (i.e. as in typical potash products), the potash bed properties can be predicted from the properties for each narrow range of particle sizes in the mixture.

Chen (2004) developed a one-dimensional transient numerical model of moisture transport accounting for diffusion, capillarity and gravity effects within potash beds. Two kinds of moisture transport mechanisms were presented, moisture transfer caused by liquid film movement due to capillarity and gravity effects in a wet region where local moisture saturation level, *S*, is larger than an irreducible saturation, S_0, and water vapour diffusion and water adsorption in layers on the surfaces in a dry region where *S* is less than S_0. The moisture content spatial distribution for different particle sizes under different initial conditions was also measured using an experimental facility. Both experimental data and numerical simulation results showed that the irreducible saturation is a strong function of particle size and this property will decrease as particle size increases. This research for step changes in bed moisture content indicated that water vapour diffusion will always occur through the interstitial void spaces between particles but water drainage due to gravity will only occur when the initial moisture content exceeds the critical value for each particle size.

Moisture transport in potash beds is the essential factor to cause caking problems in potash products. These research studies on the heat and moisture transfer processes in potash provided valuable data and theoretical/numerical models so that one can understand the mechanism of moisture accumulation, salt dissolution and moisture movement in a humid environment. No studies were done on the caking process resulting from recrystallization during drying and no direct measurements of the cake strength were taken, nor were fracture stresses calculated.

1.3.2 Cake strength studies for bulk materials

Since the 1930's, many papers and reports have been published concerning the handling, caking and application of bulk materials such as potash. Rumpf (1958) reviewed agglomeration phenomena, including both desired phenomena such as granulation and the formation of large particles from small ones, or undesired phenomena such as when cakes form in bulk granular materials which are intended to retain free flowing characteristics. He also presented a synopsis of the various bonding mechanisms. For the bonding mechanism with material bridges, Rumpf suggested the investigation of the tensile strength of agglomerates to gain a fundamental understanding using comparable data. He developed a theoretical equation for the tensile strength of agglomerates bonded together in a bed of mono-sized spherical particles.

Guided by Rumpf's theory and using a salt particle range of 15 μm to 60 μm, Pietsch (1969) investigated the correlation between the drying behaviour and the tensile strength of limestone agglomerates bound together by NaCl salt bridges in the dry state. In this experimental study, limestone powders were wetted with a selected amount of NaCl-solution and were pressed into cylindrical green pellets 30 mm in diameter. Each sample was dried in an oven and machined to remove the crust layer which was about 2 mm thick. The tensile strength of these dry pellets was measured by using a specially constructed tensile strength tester. The mean particle size of the limestone powders, the initial percentage liquid saturation, the salt concentration of the solution and the drying temperature were varied as independent parameters in a series of experiments. It was stated that the tensile strength of the dry pellet depends on the quantity and the local distribution of the crystalline salt on the surface.

Thompson (1972) presented a comprehensive review and experimental study of the caking process in typical granular fertilizer products. He investigated the relationship between caking of the granular fertilizer and moisture content, storage pressure, temperature and time using a special laboratory cake strength apparatus. Each sample was caked in a shallow mould and the differential pressure over the top and underneath of the mould required to remove the caked sample in the mould was taken as a measure of degree of cake. Experimental results revealed that these factors are all necessary to create any significant cake. For ammonium nitrate prills he concluded that caking is primarily brought on by a deformation process based on plastic creep. According to Thompson these high pressure contact areas between prills are bound together by a surface tension the pressure deficiency beneath a curved meniscus of the aqueous film between prills. The long-term storage trail where the cake was measured in exposed plastic bags subject to a drop test at the end of the test duration would be advisable to confirm the results of laboratory tests.

Tanaka (1978) developed a theoretical model of a cake fracture stress in a caked particle bed comprised of spherical particles in contact with one another. This model was used to predict the ultimate cake strength of powder products such as NaCl. The relationships between cake strength, moisture content and drying time predicted by Tanaka indicates that the cake strength should be proportional to the square root of drying time and an exponential function of the initial moisture content before drying.

Walker et al. (1998) investigated the caking process for mixed granular nitrogen, phosphorus and potassium fertilizers for accelerated cake tests to determine the role of unbound water, and the effect of ammonium chloride. Compression testing using an

Instron Test System was used to determine the cake strength of NPK fertilizer. They indicated that the caking process is dominated by the accumulation and movement of free water by capillary adhesion culminating in a crystal bridging process. Water at the contact points is essential to cause caking. This investigation suggested that the presence of free water on the surface of the granules causes mass transfer of saturated fertilizer salts to the granule surface where solid crystal bridges can form upon evaporation. Walker et al. (1999) continued the research work on the caking phenomenon in fertilizer products. Their plastic creep-capillary adhesion model based on empirical correlation was developed to predict the caking propensity of granular fertilizers considering the increased granule-granule contact area caused by plastic creep. They found that the cake strength increases with the increased steady-state creep rate, which is a function of storage pressure.

Arinze et al. (2000) experimentally determined the relationship between moisture content and a qualitative degree of caking. They further investigated (Arinze et al., 2001) the factors that influence caking such as the environmental humidity and temperature, moisture content, storage pressure, handling impact velocity and storage time and developed empirical correlations for the onset of caking.

1.3.3 Cake strength measurement

In the past, several methods have been investigated to assess the cake strength in potash fertilizer samples. These methods can be grouped into two categories: comparative and quantitative methods. The Potash Corporation of Saskatchewan cake measurement method is a typical comparative method to measure cake strength (Arinze

et al., 2000 and 2001). In this method, a caked potash sample is placed on top of a standard screen mounted on a vibrator and the screen is vibrated for 10 seconds. Compared to the initial mass the fractional mass of the sample retained on top of the screen after this vibration is used to determine a comparative caked fraction. Empirical results presented using this method are only meaningful when a large data base of comparative samples are developed. This method of testing has proved to be useful in evaluating the performance of various types of anti-caking agents added to the external surfaces of potash particles.

In order to better quantify the mechanical cake strength of bulk samples, various test devices have been used which may be classified as shear, compression and tensile test methods. Shear type loads occur in granular bulk fertilizer piles when bulk materials are moved by sliding the bulk material over surfaces or through hoppers. The shear cake strength of granular bulk fertilizer, such as potash, has been characterized using the Jenike Shear Tester, a device in which a caked cylindrical shaped sample is sheared in half by a shear force while a normal axial force is applied on the sample (ASTM Std. D6128-00, 2003; Kollmanu and Tomas, 2001). Compression type loads occur in bulk fertilizer storage piles due to the hydrostatic weight of the bulk material above any point inside a storage pile. A compressive test method was used by Walker et al. (1999) to investigate the cake strength in cylindrical caked fertilizer specimens similar in geometry to that specified to test concrete cylinders (ASTM Std. C39/C39M-03).

These methods all require relatively complex models to determine the stress at failure and this leads to large uncertainties in the data even when the auxiliary external

loads are carefully controlled. For example, shear testing with the Jenike Shear Tester requires the user to apply a force normal to the shear plane along the axis of the test cylinder and another force parallel to the shear plane across the cylinder in a test cell of caked material. Since the force normal to the shear plane is selected on the basis of empirical data, it adds complication to the stress analysis and results in large compressive and shear stresses as well as local tensile stresses at the shear plane.

A tensile tester was used to measure tensile strength of caked sugar (Leaper et al., 2002). In this technique, caked material was bonded to the surface of a split cylinder whose two halves are pulled apart by a tensile force. The applied force at fracture divided by the fracture surface area gives the tensile strength of the specimen cake. Leaper investigated the caking effects of repeated exposures to cycles of ambient air relative humidity between 70% and 20% by measuring this tensile strength for many samples of caked materials. They found that, as the number of specimens increased, a large variation in the tensile strength occurred. These results suggest that bonding variations between sample and cell surfaces and the inconsistent position of the fracture surfaces help to explain the significant variations in the experimental data for the calculated failure tensile strength.

In both the Jenike shear test cell and the Leaper tensile test cell, an attempt was made to force the sample failure surface to occur on a unique predetermined fracture surface in each sample. This implies that the sample cake characteristics are homogeneously distributed throughout the cell. In the test results of Leaper et al. (2003), the stress field is uniform but the fracture surfaces are non-planar suggesting that the assumption of homogeneity is not valid, even when care is taken to create test samples

with homogeneous properties. Although the compression test method of Walker et al. (1999) does not depend on predetermined failure surfaces with each sample, it results in stresses in each test sample with complex compression, tension and shear components that vary radially and axially throughout each sample.

1.3.4 Recrystallization process and moving boundary problems

Drying and caking in a bed of granular fertilizer during bulk storage are complex chemical-physical processes. Most of the earlier investigations hypothesized that crystal growth during a drying process may be a prime cause of caking. Kollmann and Thomas (2001) showed a microscopic photo of what they claim is a crystal bridge in their study of cake formation (Figure 1-5). In the past, recrystallization process which is a problem with phase change and moving boundaries had been investigated experimentally and numerically.

A simple tension testing method was used by Sun et al. (2006) to determine the fracture tensile stress of pairs of specially prepared caked sodium chloride and potassium chloride particles. In their study, NaCl and KCl particles, of 99% purity and 15 mm to 20 mm size, were cut into two pieces of approximately equal size by a diamond saw to obtain smooth contact surfaces. The paired pieces of NaCl and KCl were placed in contact and exposed to a cavity filling wetting, followed by a drying process. After recrystallization, the fracture tensile stress for the caked particles was measured. The surface roughness of contact areas was measured before and after testing. Typical experimental results showed that the area-averaged tensile stress for these NaCl and KCl particles was 330 KPa which is only a very small fraction of perfect molecular

bond strength for NaCl or KCl (i.e. 11.5 GPa for KCl and 15.2 GPa for NaCl). It was also found that contact surface roughness of the original fracture surface area was 5 times larger after drying than that measured before wetting. These results imply that only a very small fraction of the salt particle surface contact area is bonded or caked together. Sun et al. (2006) suggested that although large crystals form everywhere on the surface only a very few crystals develop contact points between the particles during recrystallization. Microscopic image analysis of an original cut surface shows that the largest crystal sizes formed during recrystallization were 1 to 2μm. Based on these experimental findings, it can be concluded that only the region very near contact points between particles in a particle bed are important for caking. During a caking process between particles, only the crystals which are deposited very near contact points have the potential to fill the gap between particles so that crystal bridges could form to bond particles together. Outside these contact point regions the distance between particles in a bed is larger than the crystal growth so no crystal bond can be formed between particles during recrystallization.

Models of phase change with moving boundaries are called Stefan problems due to his 1891 paper which correctly formulated the non-linear problem of phase change from liquid to solid in a infinite domain with only one important dimension (Carlslaw and Jaegar 1959, Yao and Prusa 1989). Muller-Krumbhaar (1975) considered this Stefan problem for planar crystal growth surface due to transport of solute near a moving crystal-liquid interface. He used several different perturbation methods of solution to investigate the influence the solute concentration on crystal growth for various cases with equilibrium and non-equilibrium boundary conditions, constant

cooling rate and temperature dependent diffusion coefficient in a semi-infinite domain. Assumptions for this study included one dimensional effects, uniform temperature and negligible gravitational effects. Crank (1984) has presented a detailed account of the mathematical solution of moving boundary problems and reviewed the numerical algorithms used to solve these problems. Wang and Hu (1999) numerically investigated the concentration distribution for a quasi-steady state of solution crystal growth in a two-dimensional rectangular container in a low gravity environment. They showed that it was important to include the moving crystal growth interface because it influences the concentration distribution in some cases.

Some research has been done to predict the deposition of a dissolved salt in a liquid when the liquid water evaporates into a dry particle bed of soil and diffuses to the top surface of the soil (Tsypkin and Brevdo, 1999).

1.4 Research Objectives

It is well understood that the initial moisture content in potash products is an essential factor to influence the cake strength of granular potash but other factors such as particle size, temperature and bed pressure also appear to play a role according to the literature on moisture transport and caking. Several research works have been carried out to try to determine the quantitative relationship between cake strength and these factors using different cake strength measurements. As discussed above, one of the difficulties in establishing such a relationship between cake strength and the above variables has been the lack of an accurate test method.

It is also clear from the literature that the physical phenomena associated with cake formation in particle salt beds, such as potash, are not entirely understood in spite of the well known physical principles and chemical properties of electrolytic solutions. This dearth of a good theoretical model, which has been partly a consequence of insufficiently accurate cake strength data and controlled test methods, has led researchers to list and correlate many factors that appear to influence caking when in fact there are maybe only a few important factors. There is a need to model and simulate these primary factors that influence caking and to compare these predictions with more accurate cake strength data.

Therefore, a new experimental method which can measure cake strength of the caked potash sample with a high accuracy and the theoretical/numerical model to simulate/predict the caking process around contact points between particles would be of great practical significance. The primary factors such as initial moisture content, particle size, drying time and chemical composition on particle surfaces need to be tested using a new experimental method. Data from these tests should be compared with the prediction by the developed numerical model of recrystallization near one contact point between two potash particles during drying process. The main objectives of this research are:

(1) To develop a new test method to accurately measure the fracture strength of caked potash samples.

(2) To investigate and quantify the effects of initial moisture content, drying process, particle size and chemical impurities on the strength of caked potash test samples using the new test method in (1) and specify the uncertainty in these data.

(3) To develop an analytical/numerical model for the caking process near the contact points between particles in a test sample.

(4) To investigate the caking process with the numerical model in (3) by varying significant physical effects such as initial moisture content, evaporation rate and supersaturation on each particle surface.

(5) To compare the numerical model predictions in (4) with the measured cake strength data from (2).

In order to achieve these objectives, a number of steps are required to measure the cake strength of a caked potash sample and develop the theoretical/numerical model of recrystallization near one contact point between two potash particles during a drying process. These specific steps include:

(1) Devise and design a new test facility that can be used to measure the fracture cake strength of specimens such that the test results in a symmetrical stress field which is predominately tensile but has no specific fracture plane. Develop a mathematical model for the stress distribution at the condition of sample fracture.

(2) Prepare test samples for a range of test conditions by changing the key parameters such as: initial moisture content, particle size, drying time and chemical compositions (i.e. magnesium content) of potash particles. Measure the cake strength and explore the relationship between cake strength and these factors. Determine the uncertainty in these data for each set of tests.

(3) Theoretically formulate and numerically model the recrystallization process due to thin film evaporation on wetted salt particles close to one contact point between two particles. Simulate the mass distribution of recrystallization near this contact point to investigate the effects of the initial thickness of the liquid film electrolytic layer (i.e. initial moisture content), velocity of moving liquid film-air interface or rate of drying, and the degree of supersaturation on the solid surface near the contact point.

(4) Compare the simulated results of mass deposition near a contact point with previously measured cake strength in sample test beds of potash. For various parameters used in this numerical model, investigate the sensitivity of the important properties.

1.5 Overview of Thesis

A centrifugal loading method to measure the cake strength in a caked potash ring is described in Chapter 2. The details of the test apparatus, test sample preparation and measurement techniques are presented in this chapter. A stress analysis is also presented relating the speed of the centrifuge to when the specimen fractures. The cake strength is measured for the tests in which the initial moisture content and drying time of each sample is varied.

Chapter 3 presents the experimental data obtained during a series of tests in which the initial moisture content, particle size, drying duration and chemical content of particles are varied. The relationship between cake strength and these factors are shown in this chapter along with the uncertainty analysis of the data and the correlations used.

Chapter 4 develops a theoretical/numerical model to simulate ion diffusion and crystallization near one contact point between two potash (KCl) particles during a typical drying process. This model can be used to examine the recrystallization process between potash particles as a result of water evaporation after the particles have been previously wetted.

Chapter 5 investigates the effects of three independent factors on the caking process: initial moisture content; evaporation rate and degree of supersaturation on the surrounding surface. Qualitative agreement between simulated results and measured experimental fracture stress data is investigated in this chapter.

In Chapter 6, the summary and conclusions of this research are presented. Several recommendations and suggestions for future work are proposed.

The appendices includes: (1) Experimental measurement of the bond strength between the caked potash and a PVC plate; (2) Measurement of elastic properties for a caked potash sample; (3) Measured experimental data for cake strength; and (4) Sensitivity studies on parameters used in the numerical model.

CHAPTER 2

MEASUREMENT OF CAKE STRENGTH IN POTASH USING A CENTRIFUGE

2.1 Background

Accurate measurement of cake strength is of great importance to understand the caking process for bulk fertilizer products and it may also have a practical value for quality control. In the past, the caking behavior of potash fertilizer products was characterized using several different test methods including qualitative measurement such as the PCS comparative measurement method (Arinze, 2000) and quantitative measurements such as the Jenike Shear Test method. The comparative method provides empirical results for a large data base of different quantitative samples. The Jenike test method results in three dimensional strain effects that cause large uncertainties in the data.

Textbooks on fracture mechanics (e.g. Craig, 2000; Felbeck and Atkins 1984) state that the failure mode of brittle materials will be primarily caused by tensile stresses, and not by compression or shear stresses at the fracture surface. This would suggest that caked particle test samples should be loaded in such a manner that the tensile stresses dominate. However, due to the somewhat random nature of the caking properties in

particle beds, no attempt should be made to predetermine the location of the failure surface inside a caked sample.

One device that can produce this type stress field is a centrifuge. In this research, the fracture cake strength of potash will be measured using this new method that results in symmetrical stresses that are predominately tensile. This device can be used to find the relationship between the cake strength in a potash bed and its initial moisture content, drying time, particle size and chemical composition of particles.

The strength of cake bonds between particles may be compared to the strength of pure crystals, but the surface area of the contact points between the particles in a packed bed is many orders of magnitude smaller than the cross-sectional surface area of the bed. When caking occurs this results in a low, but significant, area-averaged fracture strength caused by the chemical bonds between the particles near their contact points within a caked bed of particles. As mentioned previously, brittle materials, such as caked potash, usually fail in tension. Because crystalline caked potash is a brittle material, a tensile stress induced failure is expected to be the most likely mode of failure. With such a brittle material the ultimate fracture cake strength is best determined using a test specimen under tension with little or no asymmetries or stress concentrations on the boundaries of the specimen.

A centrifuge was used to create the internal tensile stress field in a ring specimen of potash particles in a caked sample subjected to a constant rotational speed. The continuum method of stress analysis in a two-dimensional plane-stress ring is used to calculate the area-averaged tensile stress required to fracture a caked potash sample.

This method of analysis assumes that the caked specimen is a continuum with homogenous and isotropic properties. In this method a two-dimensional, plane-stress, elastic stress-strain field with a finite radial stress on the inner surface boundary is considered. This results in a slightly non-uniform tensile stress distribution on any radial cross-section of the specimen.

In this chapter, a detailed description of experimental facilities and test procedure is presented. The stress analysis at the sample fracture and the calculation of area-averaged fracture tensile stress (i.e. cake strength) are presented. The cake behaviour of potash for one particle size range from 0.85 mm to 1.18 mm is evaluated first for various initial moisture contents and drying procedures using this method.

2.2 Test Principle

Figure 2-1 shows a schematic of the plastic ring and bottom plate used to hold each test sample during a test. These surfaces are both in contact with the potash crystal during the preparation of each test sample and during each test in the centrifuge. The caked potash samples were made using an annular ring device which is mounted on a centrifuge and can be rotated at continuous speeds from 0 to 1000 rpm.

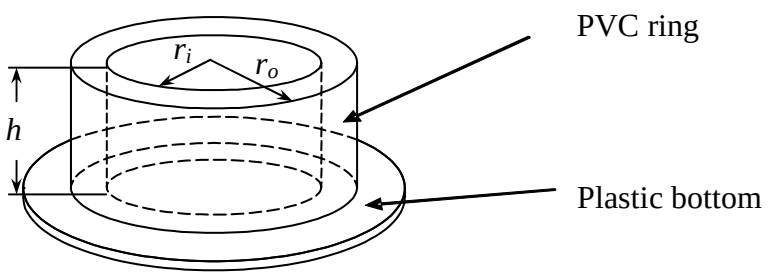

Figure 2-1: Plastic ring and bottom plate used to hold a caked potash sample

Figure 2-2 (a) is a photograph of the annular ring which is configured for caking preparation between the two concentric rings and Figure 2-2 (b) is a photograph of a prepared cake. The cylindrical height, h, of each sample tested was 27 mm, the sample wall thickness, (r_o-r_i), was 12 mm, and the radius of the inside radius, r_i, was 65.5 mm. The test cell is made up of a horizontal circular plastic base upon which sits a plastic tube, which is surrounded by a removable outer circular plastic cylinder as shown in Figure 2-2 (a).

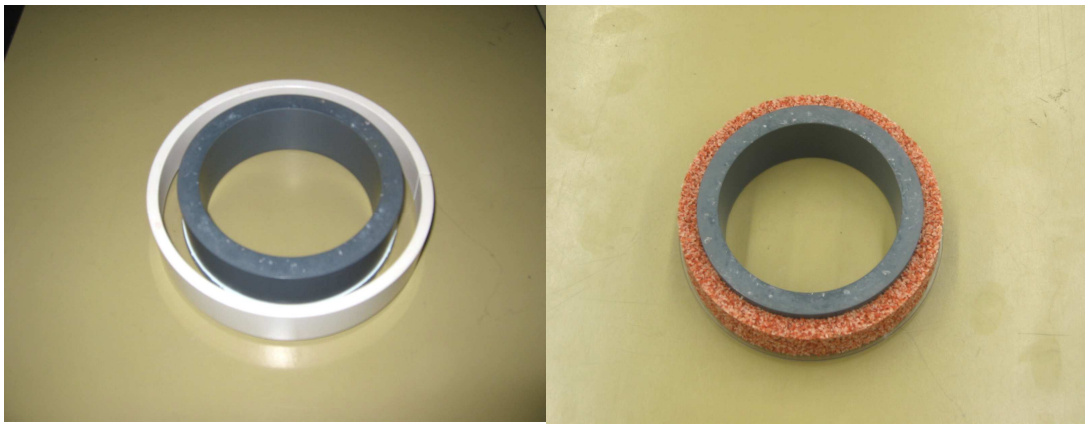

(a) (b)

Figure 2-2: Photos of (a) plastic annular ring device to make caked potash samples and (b) prepared caked potash sample with its holder for testing in a centrifuge

2.2.1 Stress analysis in a 2-D plane-stress ring

The geometry of the caked potash sample in a packed bed of particles with known uniform and isotropic properties of porosity and density is assumed to be a symmetrical cylindrical shell. Figure 2-3 shows a schematic of a 2-D ring of potash and

a free body element inside this 2-D ring which has no stress in the *z*-direction normal to the *r*-θ plane (i.e., this is the case of plane stress at every point in the sample ring).

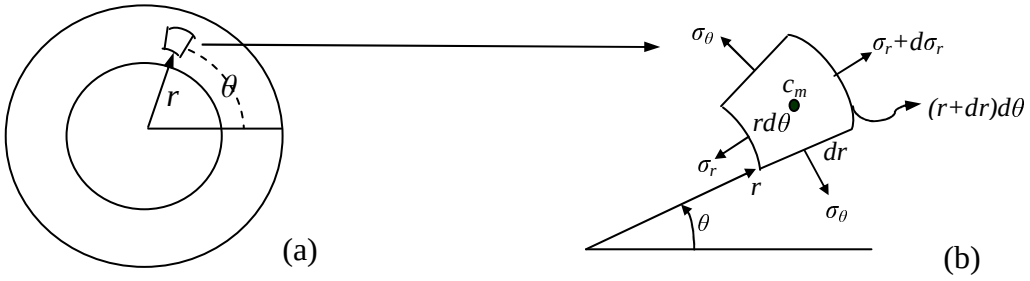

Figure 2-3: Schematic of (a) axisymmetric rotating caked potash cylinder and (b) stresses on an infinitesimal element at *r*, θ

A differential analysis is used to determine the tensile stress in the sample at a given angular speed. It is assumed that the caked potash is a continuum in the sample ring which undergoes symmetrical plane stress in *r*-θ and certain selected boundary conditions apply at $r=r_i$ and $r=r_o$.

The elastic relationship between stress (σ) and displacement (u) at any point (r, θ) in the sample ring is given by (Budynas, 1999):

$$\sigma_r = \frac{E}{1-\nu^2}\left(\frac{du}{dr} + \frac{\nu u}{r}\right) \qquad (2\text{-}1)$$

$$\sigma_\theta = \frac{E}{1-\nu^2}\left(\frac{u}{r} + \frac{\nu du}{dr}\right) \qquad (2\text{-}2)$$

For an equilibrium force balance on the infinitesimal element in Figure 2-3(b) at constant angular speed, ω, and body force acceleration, $r\omega^2$, the displacement equation is:

$$\frac{d^2u}{dr^2}+\frac{1}{r}\frac{du}{dr}-\frac{u}{r^2}=-\frac{1}{E}(1-\nu^2)\rho r\omega^2 \tag{2-3}$$

Solving this non-homogeneous and linear ordinary differential equation and using the definition of tangential stress and radial stress in equations (2-1) and (2-2) gives the stress components at any point inside the test specimen:

$$\sigma_r = C_1+\frac{C_2}{r^2}-\frac{(3+\nu)}{8}\rho\omega^2 r^2 \tag{2-4}$$

$$\sigma_\theta = C_1-\frac{C_2}{r^2}-\frac{(1+3\nu)}{8}\rho\omega^2 r^2 \tag{2-5}$$

where C_1 and C_2 are coefficients of integration which are determined from the boundary conditions presented in section 2.2.2 and are related to the rotational speed, ω. The mean radius of the cylindrical test sample shell, $r_m=(r_o+r_i)/2$, is used as a characteristic radius. The dimensionless forms of σ_r and σ_θ are:

$$\xi_r = C_1{}'+\frac{C_2{}'}{\psi^2}-\frac{(3+\nu)}{8}\psi^2 \tag{2-6}$$

$$\xi_\theta = C_1{}'-\frac{C_2{}'}{\psi^2}-\frac{(1+3\nu)}{8}\psi^2 \tag{2-7}$$

where $\xi_\theta=\frac{\sigma_\theta}{\rho\omega^2 r_m{}^2}$, $\xi_r=\frac{\sigma_r}{\rho\omega^2 r_m{}^2}$ and $\psi=\frac{r}{r_m}$

$$C_1{}'=\frac{C_1}{\rho\omega^2 r_m{}^2},\ C_2{}'=\frac{C_2}{\rho\omega^2 r_m{}^4}$$

For a radial fracture section the dimensionless area-averaged tensile hoop stress is defined as:

$$\bar{\xi} = \frac{1}{\psi_o - \psi_i} \int_{\psi_i}^{\psi_o} \xi_\theta \, d\psi \qquad (2\text{-}8)$$

2.2.2 Boundary conditions

In order to analytically solve the equation for stress in the caked potash shell under a centrifugal force, the boundary conditions at the inner surface and outer surface must be specified. The tensile hoop stress and radial stress distributions will be determined subject to these boundary conditions.

For the outer surface of the caked potash shell which is exposed to air, the dimensionless radial stress is zero (i.e. $\xi_r \Big|_{r = r_o} = 0$).

For the inner surface, the caked potash is bonded to the PVC ring. The boundary condition at this surface needs special consideration. The displacement of the inner surface of caked potash is not expected to be exactly zero when the angular speed is finite but, for the low speeds used, it will be very small. This potash-PVC interface cannot support a large stress because potash does not bond well to smooth plastics and, for a given volume of bulk material, the number of particle-plastic surface contact points is much smaller than the number of contact points between particles elsewhere in the bed. At the instant of fracture it is expected that the radial stress on the plastic surface, compared to the tensile hoop stress, should be small. The area-averaged tensile stresses are many orders of magnitude smaller than the stresses that can exist in perfect chemical

bonded crystals and the number of contact points between particles per unit volume of bed which form strong chemical bonds in caked potash is the important factor in determining the ultimate area-averaged stresses in a caked bed. A higher number of contact points between particles per unit volume imply a larger contact point area per unit volume and a stronger cake strength or ultimate stress. Figure 2-4 shows a two-dimensional schematic of spherical particles in a caked specimen ring showing typical contact points at a typical fracture surface between spherical particles (b) and on the inner bed PVC- surface interface (c).

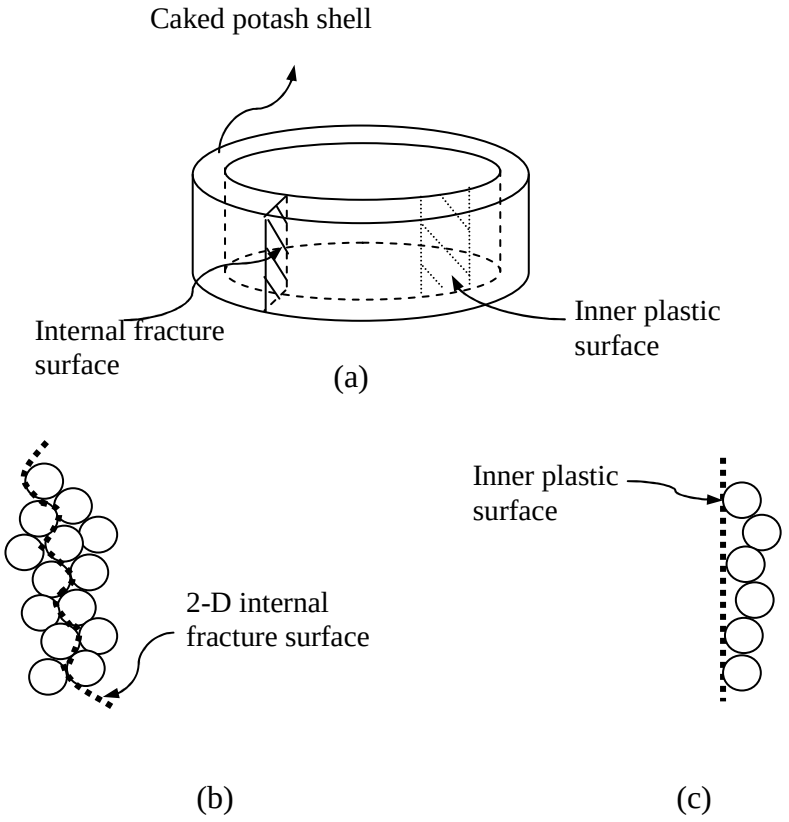

Figure 2-4: Schematic showing (a) caked potash shell specimen, (b) particle contact points on an internal fracture surface, and (c) fracture surface between the particles and the PVC surface

Kaviany (1999) suggested a range of 6-12 contact points per particle for a typical bed of nearly spherical particles. Potash particles, with an irregular crystalline shape, may have a few more contact points per particle in a packed bed. A range of particle sizes in a packed bed of particles will increase the number of contact points per unit volume and when caked, the strength of the cake could be larger. As well, the existence of very fine dust like particles attached to the larger particles will increase the surface area per unit volume and potentially increase the cake strength. At the inner surface of the caked test sample ring, there will be only one contact point per particle on the PVC surface. Also, the strength of the chemical bond between particle and PVC material will most likely be much smaller than the crystal-to-crystal bonds so it may be concluded that the stress at the inner plastic surface will be much smaller than elsewhere. Therefore, a small value of radial stress on the inner surface of a caked potash shell is estimated to be a small fraction of the average tensile stress. Using this boundary condition, the coefficients C_1' and C_2' in equations (2-6) and (2-7) are determined and the stress distribution is determined. In appendix A, a simple test is presented to measure the bond strength between caked potash and PVC plate. The experimental results show that bond strength between potash and PVC material is about 400 times smaller than the tensile fracture stress for any of the centrifuge tests.

In this research, the radial stress at the inner surface of the caked potash ring is assumed to be zero (i.e. $\xi_r \big|_{r=r_i} = 0$). A sensitivity study of this boundary condition is also presented by selecting very small stress on this boundary (i.e. $\xi_r \big|_{r=r_i} = \xi_c$ where $\xi_c = \sigma_c / \rho\omega^2 r_m{}^2$).

2.2.3 Stress distribution

The Poisson's ratio, ν, of caked potash sample was measured using a cylindrical compression test specimen and an INSTRON tester, which is described in Appendix B. This test determined Poisson's ratio to be about 0.10. Before solving the 2-D plane-stress model, another method of stress analysis was considered by applying thin shell theory. Using fundamental solid mechanics, for a thin caked potash ring the tensile stress distribution across the caked potash sample is determined while the radial stress, σ_r, on the inner ring surface is neglected. Using this method, the tensile stress, σ_θ, is given by $\rho^2\omega^2 r_m{}^2$. Compared with the plane stress analysis method, this simplified calculation for cake strength in a caked potash bed gives a reasonable approximation for the tensile stress.

By solving the equations (2-4) and (2-5) subject to zero stress on the boundaries $r = r_i$ and $r = r_o$, the coefficients C_1 and C_2 are given by:

$$C_1 = \frac{3+\nu}{8}\rho\omega^2(r_i{}^2 + r_o{}^2) \qquad (2\text{-}9)$$

$$C_2 = -\frac{3+\nu}{8}\rho\omega^2 r_o{}^2 r_i{}^2 \qquad (2\text{-}10)$$

In fact, thin shell theory is a special case for equations (2-4) and (2-5) as r_i goes to r_o. In this case it means that $r_i \approx r_o \approx r_m$ for a thin caked potash ring. Solving equations (2-4) and (2-5) using the determined C_1 and C_2 which are subject to zero stress on both inner surface and outer surface, the tensile stress is also given by $\rho^2\omega^2 r_m{}^2$.

A more general non-dimensional form of C_1' and C_2' is given by equations (2-11) and (2-12) by considering a very small radial stress on the inner surface of caked potash ring (i.e. $\xi_r\big|_{r=r_i} = \xi_c$). A sensitivity study was carried out by selecting several small radial stresses as the inner boundary conditions.

$$C_1' = \frac{\frac{3+\nu}{8}(\psi_o^4 - \psi_i^4) - \xi_c \psi_i^2}{\psi_o^2 - \psi_i^2} \qquad (2\text{-}11)$$

$$C_2' = \frac{\xi_c \psi_o^2 \psi_i^2 - \frac{3+\nu}{8}\psi_o^2 \psi_i^2 (\psi_o^2 - \psi_i^2)}{\psi_o^2 - \psi_i^2} \qquad (2\text{-}12)$$

Figure 2-5 shows the dimensionless tensile stress distribution, ξ_θ, in a caked potash ring subjected to zero radial stress at inner boundary and two small constant radial stresses, as well as the dimensionless tensile stress distribution using the method of thin shell theory indicated by the straight line in this figure. It can be seen that the dimensionless tensile stress, ξ_θ, is nearly linear with ψ over the radius of each specimen, and the change in ξ_θ from inner to outer surface is small relative to the mean value. If the rotating speed at the fracture of sample, ω, and density of caked potash sample, ρ, are known, the dimensional stress distribution at fracture will be determined and the area-average tensile stress (i.e. cake strength) can be calculated. Therefore the measurement of rotating speed at the instant of sample fracture will establish the fracture stress in this new test experimental method.

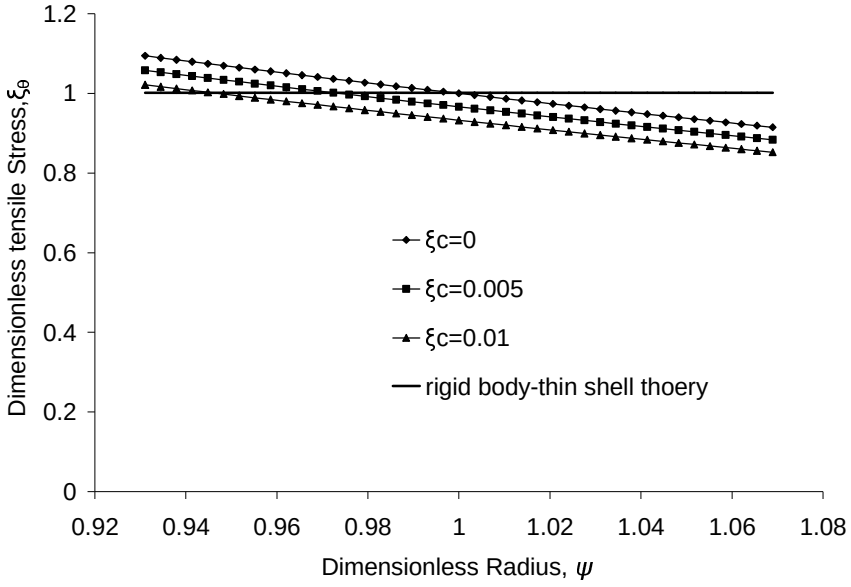

Figure 2-5: The radial distribution of dimensionless tensile stress ,$\xi_{\theta,}$ in a caked potash ring for v = 0.1 with inner radius dimensionless stress as a parameter

The sensitivity study of the inner boundary conditions also shows that the very small radial stress on the inner surface will not influence the stress distribution in the specimen significantly. Therefore, using a zero radial stress on the inner surface will give reasonable accuracy for the stress analysis. In this research, this boundary condition will be used to calculate cake strength for each test caked potash sample.

Figure 2-6 shows of Mohr's circle for plane stress in an isotropic media (Pilkey, 2005), which illustrates how the normal and shear stress components vary at every point in a test sample as a function of stress surface orientation angle, θ. The normal stresses equal the principal stresses when the stress is aligned with the principal directions (i.e. r and θ directions). The shear stress is a maximum when the surface on which stress occurs is rotated 45^{o} away from principal directions and its value equals $(\sigma_\theta - \sigma_r)/2$.

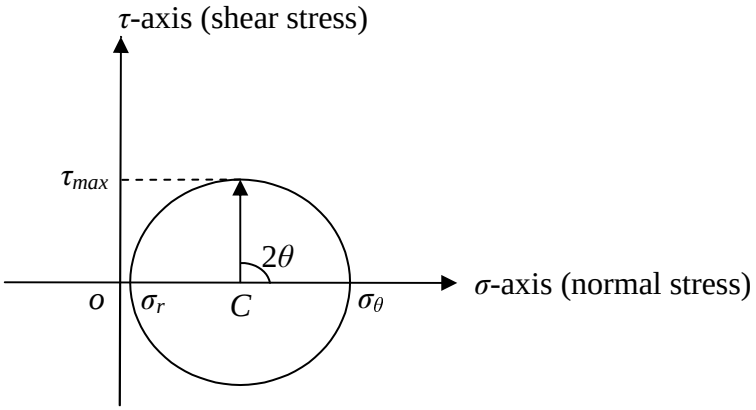

Figure 2-6: Mohr's circle diagram for plane stress in a caked potash structural element

The principal stresses are $\sigma_{\max} = \sigma_\theta$ and $\sigma_{\min} = \sigma_r$ for the symmetric ring sample and the maximum shear stress distribution over the range of radii for the case of zero radial stress on the inner boundary are shown in Figure 2-7.

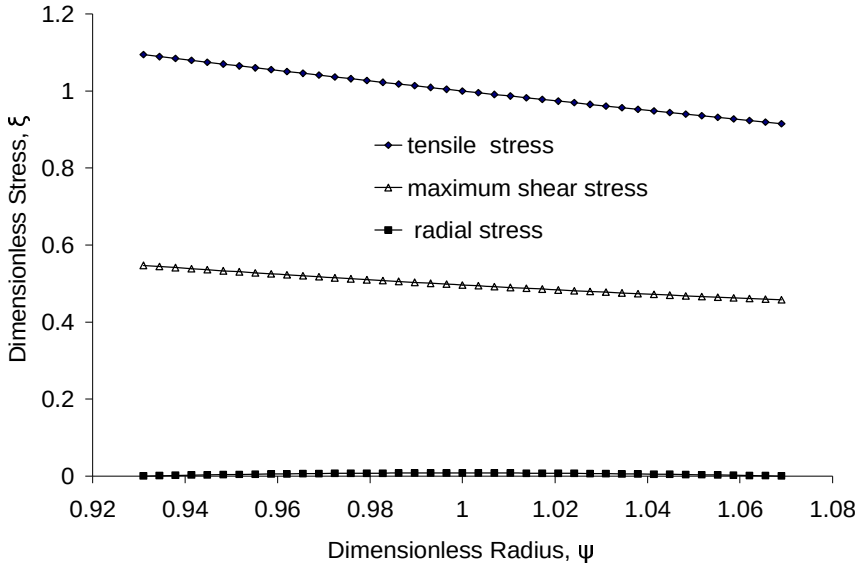

Figure 2-7: Principal stresses and maximum shear stress distribution across caked potash for a radial cross-section

It is shown in Figure 2-7 that the tensile stress field dominates across a specimen tested in a centrifuge. Based on this analysis, it is feasible to determine the cake strength by fracturing the caked sample under tension produced by centrifugal force.

2.3 Experiment

2.3.1 Sample preparation

The potash samples that were used in the experiments were selected from Lanigan standard potash produced by Potash Corporation of Saskatchewan. These samples had not been treated with anti-caking agents. Lannigan standard potash is a granule grade potash product with size ranges from 0.5 mm to 2 mm diameter. In order to reduce the uncertainty or variation caused by particle size distribution, a standard sieve series (Canadian and US) were used to sieve the granular potash particles into a narrow range of particle sizes. This was done to investigate the effect of particle sizes on cake strength. The experimental equipment to obtain a narrow particle size range is shown in Figure 2-8 including the shaker and the sieves. A sieve shaker (ROTA-SIFT) driven by an electrical motor is used to obtain the needed range of particle sizes by using the different standard sieves. The sieve shaker was operated for sufficient duration to result in a particle size distribution that was invariant with time. Firstly, a particle screening size range of 0.85 mm to 1.18 mm was used for all tests in this chapter.

Figure 2-8: Experimental apparatus for particle sieving

The sieved potash particles were firstly dried at 70 ^{o}C for 24 hours to eliminate residual moisture content. In order to prepare a caked sample of potash a known mass of water was then added to a known mass of potash and the initial moisture content was calculated. After complete mixing of the water and potash by an electric mixer, the wet potash was placed into the plastic annular ring device shown in Figure 2-2 (a). It was packed and vibrated until no more particles could be added. Then the wetted sample was dried. In this study, three different drying processes were used to investigate the effect of different drying duration on cake strength. These three drying methods are controlled relative humidity drying, oven drying and air drying. In controlled relative humidity drying, the sample was dried inside a closed container with a saturated salt solution on bottom which produces the ambient air at 52% relative humidity. This drying process typically needs a time duration of 4 days. In oven drying, the sample was dried at a controlled temperature of 40 Celsius for a time duration of 10 hours. A designed and built air drying facility used for air drying is shown in Figure 2-9. The samples

(maximum 5 samples at once) were placed on the facility and the air at room temperature and room relative humidity was forced to flow through the samples and dried the samples for about half an hour.

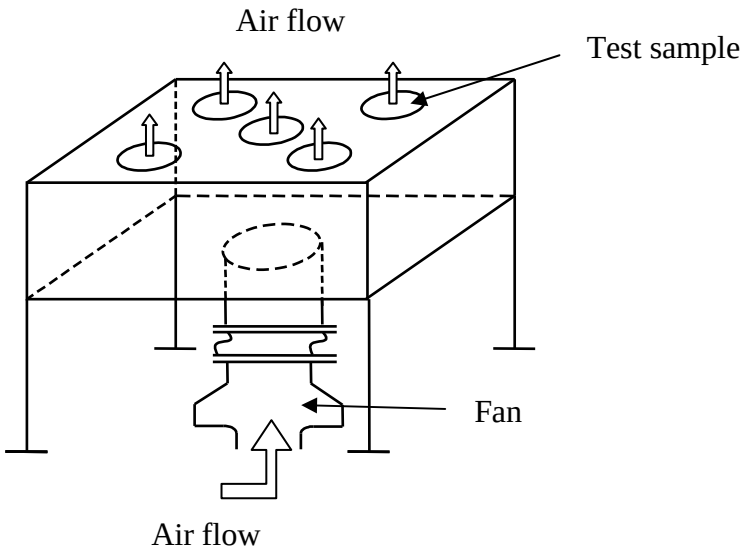

Figure 2-9: Schematic of the air drying facility which can dry five samples at once

Among the three drying processes used in this research, air flow drying resulted in the fastest drying process and the controlled relative humidity drying was the slowest. Table 2-1 shows the conditions of the three different drying methods, all with the same initial moisture content of 2.6 % (w/w).

Table 2-1: Drying Conditions for Potash Test Samples

Method	T_d (°C)	Φ_d (%)	Δt_d (hour)	V_d (m/s)
Air flow	≈22	≈20	0.25	0.3
Oven	40	≈10	10	0
Controlled R.H.	≈22	52	110	0

For the three different drying methods, Figure 2-10 shows the dimensionless moisture content versus dimensionless time for the first four time constants t_c using the exponential decay correlation $X_b / X = e^{-t/t_c}$, where t_c is the time for the dimensionless moisture content, X_b/X, to drop from 1.0 to 0.37 and the initial moisture content, X, is 2.6% (w/w).

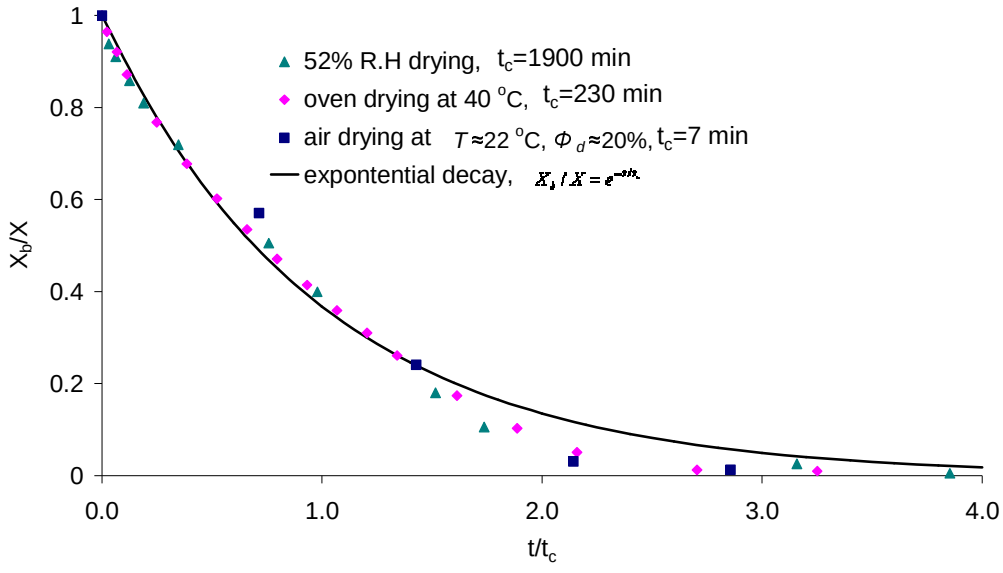

Figure 2-10: Dimensionless potash moisture content versus dimensionless time for three different drying processes

2.3.2 Experimental procedure

Once the sample had been dried, the outer cylinder was split in half and removed and the caked ring sample seated on the circular plastic base with the inner plastic ring attached was placed in the centrifuge. A special aluminium annular test cell holder had been designed and built. This device, which can be used to hold the test specimen, was assembled into the centrifuge. The test cell was attached to the holder and rotated with the centrifuge. A non-contact tachometer was used to measure the angular speed of the centrifuge. The centrifuge with the aluminium holder and the non-contact tachometer are shown in Figure 2-11.

Figure 2-11: Experimental apparatus to measure fracture rotating speed including the centrifuge, aluminium holder and non-contact tachometer

When testing, the speed of the centrifuge was increased gradually until the caked ring of potash broke and the fracture speed indicated by the tachometer was recorded. Figure 2-12 shows photos of caked potash sample mounted in the centrifuge before a

test (a) and after a test where the cake had fractured (b). The fractured ring sample inside the centrifuge outer ring indicates multiple and somewhat symmetric fracture surfaces around the test ring. The procedures for sample preparation and fracture rotating speed were then repeated for each test specimen by varying drying methods and initial moisture contents. In this experiment, the initial moisture content is varied from 0.25% to 1% for constant 52% R.H. drying, from 0.5% to 4% for oven drying and from 1% to 6% for air drying.

(a) (b)

Figure 2-12: Photos of (a) a caked potash sample mounted on centrifuge before test and (b) a fractured potash sample after test in a centrifuge

A high speed camera (30 frames per second) was used to capture the fracturing process in the centrifuge. Figure 2-13 shows photos before and after the instant fracture in a caked potash sample. Typically the caked ring specimen breaks into four pieces of nearly equal size. The fracture surfaces in the caked potash ring at the point of sample fracture are shown to be essentially flat surfaces at each of the four fracture angular

positions on the ring. Only the first fracture is important in this sequence which occurs at about the 10 o'clock position in the middle photo. The other three fractures in the ring, which occur after the first fracture, are a consequence of the stress in broken ring moving in the space between the inner plastic and outer aluminium ring. Contact of the broken ring segments with the aluminium ring causes extensive fracturing because the end state is shown in Figure 2-12 (b).

Figure 2-13: A sequence of three photos (30 frames per second) which captured the potash caked ring just before and after the instant fracture in the centrifuge, $\omega \approx 250 rpm$

2.4 Experimental Results and Analysis

Figure 2-14 shows the relationship between initial moisture content and ultimate tensile stress of caked potash bed. Each data point shown on this figure is the average of approximately 20 separate tests. The solid lines are the best fit line for all the data and the dotted and dashed lines indicate the 95% uncertainty upper and lower bonds for the linear fit using all the data.

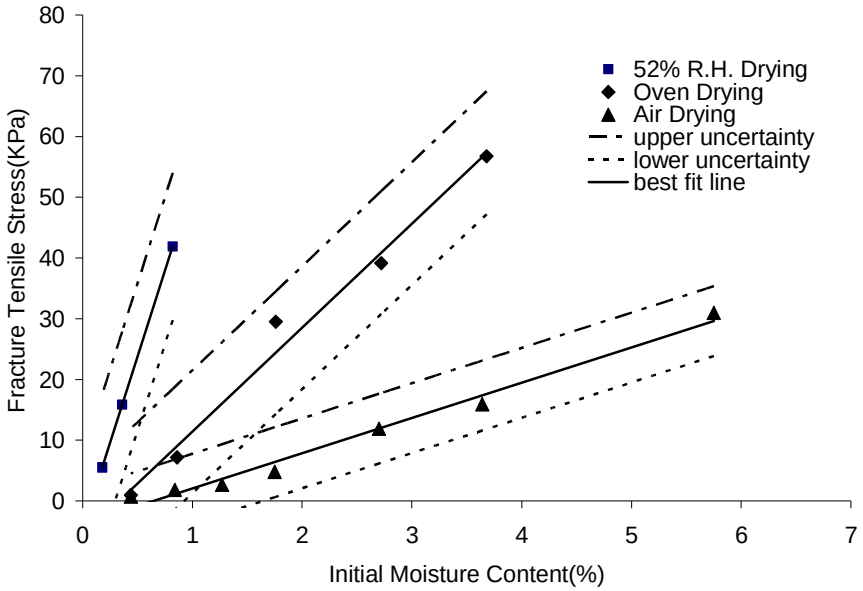

Figure 2-14: Ultimate fracture tensile stress versus initial moisture content showing average data points with three drying processes, d_{pm}=1.02 mm

These data show that the cake strength is repeatable and increases linearly with initial moisture content for each drying process. With greater initial moisture contents there is a thicker film of solution on the particle surfaces. Thicker initial films or higher moisture contents leads to more crystal bonds formed between particles after drying. This figure also shows that each potash specimen will have an increasing cake strength with longer drying processes for the same initial moisture content. For rapid drying processes, fewer ions have the time to move towards to the contact points between the particles in each specimen and this leads to fewer crystal bonds between particles during recrystalliztion. These experimental results do not agree with the cake strength model developed by Tanaka (1978). Tanaka predicted the cake strength should be proportional to the square root of drying time and should be an exponential function of initial moisture content. Our data imply that the cake strength will increase linearly with initial

moisture content. As well, the magnitude of the cake strength predicted by Tanaka does not agree with the test data shown in Figure 2-14.

2.5 Summary

In this chapter, a new centrifugal loading method has been presented. This test facility was used to measure cake strength in caked potash ring specimens and to determine the area-average tensile stress at the speed of the centrifuge when each specimen fractures. A two-dimensional elastic stress analysis is presented to calculate the area-average fracture tensile stress

Stress analysis shows that the maximum stress at any centrifuge speed at any point in the caked test rings will be tensile normal to an area element that has a vector direction parallel to the ring tangent. Fracture mechanics of brittle materials, such as caked potash, indicates each specimen will fail in tension. The location of the starting point of this failure of the ring could be at any angular position on the ring specimen.

The cake strength is measured for a series of tests in which the initial moisture content and drying time of each sample were systematically varied. For each experimental condition, approximate 20 separate tests were repeated and the 95% uncertainty for the linear fit of measured stress data was calculated using all the data for each similar test condition. Repeated experimental tests show the feasibility of this new centrifugal test method to determine the cake strength for potash samples with small uncertainties. The experimental results show that the cake strength increases linearly with greater initial moisture content and slower drying processes produce stronger cakes.

CHAPTER 3

EFFECTS OF PARTICLE SIZE AND CHEMICAL COMPOSITION ON CAKE STRENGTH

3.1 Introduction

It is understood that potash fertilizer, as a strong electrolyte, will dissolve to form a solution which consists of potassium ions (K^+), sodium ions (Na^+), magnesium ions (Mg^{2+}) and chloride ions (Cl^-) due to a mix crystal of sylvite, with small amount of halite and carnallite. These salts are hygroscopic with deliquescent relative humidities of about 52% for carnallite, 75% for halite, and 85% for sylvite. Any subsequent drying process, due to ambient air temperature increases and humidity decreases, causes growth of crystal bridges at or near contact points between particles. The formation of cakes or the recrystallization of salts near or at the contact points between particles depends on the rate of drying and chemical composition of the salt solution on the surfaces of the particles. The cake strength or fracture stress of a dried sample specimen is expected to increase with (i) the number of contact points per unit volume between the potash particles (i.e. this fracture stress will increase with decreasing particle size), (ii) the initial moisture content before drying and inversely with the drying rate (i.e. the faster the drying process the weaker the fracture strength) and (iii) increasing fractions of

magnesium or carnallite content in the dried sample. In this chapter, the experiments are carried out to quantify these relationships.

There are two purposes in this chapter: (1) to confirm and extend the data base for the relationship between cake strength and initial moisture contents before drying and to include a range of particle sizes of potash; (2) to explore the relationship between cake strength and chemical compositions (i.e. magnesium content) of potash particles. The uncertainty in the data is to be determined for each set of tests.

3.2 Test Conditions

3.2.1 Particle sizes

Samples were tested with four different ranges of particle diameter with a magnesium content of about 0.02%. The facilities and procedure to obtain a narrow range of particle size were described in Chapter two. The combinations of different sieve mesh size series were used to prepare four different ranges of particle diameter which are shown in Table 3-1.

Table 3-1: Untreated potash particle size for tests

	Range 1	Range 2	Range 3	Range 4
Particle size d_p(mm)	$0.85 < d_p < 1.18$	$1.18 < d_p < 1.68$	$2.00 < d_p < 2.36$	$2.80 < d_p < 3.35$
Mean particle diameter d_{pm}(mm)	1.02	1.43	2.18	3.08

3.2.2 Magnesium content

Samples were tested with three concentrations of magnesium on the external surfaces of the particles for one particle size range 0.85 mm to 1.18 mm (i.e. standard potash). The calculated amount of $MgCl_2$ salt was added to the standard potash and the three magnesium contents of particles were obtained: 0.02, 0.06, and 0.10 % Mg. These magnesium contents do not include the mass of Cl added.

3.2.3 Initial moisture content and drying methods

Each different type of potash was tested at three different moisture contents which were selected in the range from 0.5% to 3%. For all types of potash and all initial moisture contents, two drying methods were used to make caked samples: oven drying at 40 Celsius and air drying at room conditions.

3.3 Data and Analysis

3.3.1 Uncertainty calculation

In this chapter, all experimental data are presented by a mean cake strength, σ_{mean}, of at least twelve samples tested and with the uncertainty interval for 95% confidence. Only uncertainty resulting from random errors due to variations in the test data is considered in the uncertainty analysis of this experiment because calibration errors are negligible. Random sample errors are mainly introduced by the process of caked potash sample preparation. The estimate of the standard deviation of sample mean, S, is given by (ASME PTC 19.1, 1998),

$$S(\sigma_{mean}) = \sqrt{\frac{1}{N}\sum_{k=1}^{N}\frac{(\sigma_k - \sigma_{mean})^2}{N-1}} \quad (3\text{-}1)$$

where the mean value of the samples is defined as

$$\sigma_{mean} = \frac{1}{N}\sum_{k=1}^{N}\sigma_k \quad (3\text{-}2)$$

where, σ_k is measured cake strength for a sample of $(\sigma_1, \sigma_2, \ldots . \sigma_N)$

σ_{mean} is the mean value of cake strength

N is the number of test samples

k is k^{th} measurement

The uncertainty in the sample mean value at the 95% confidence level is defined by,

$$U(\sigma_{mean}) = t \cdot S \quad (3\text{-}3)$$

where t is the student "t" statistic which has a value of 2.1 for $N \geq 15$ tests

S is standard deviation of sample mean.

To reduce uncertainty in the measurement of cake strength, special attention was used to ensure consistent mixing and packing methods for each sample and the number of repeated tests was selected to result in a small uncertainty at each test condition.

3.3.2 Comparison of new and recycled potash

Before testing could begin on the different particle sizes and the magnesium contents of potash, the difference, if any, between particle samples as received from the mine, and recycled samples had to be determined. These tests were performed on the 0.85 mm ~ 1.18 mm diameter potash for two different drying methods; air drying from an initial moisture content of 2.80 % and oven drying at 40 Celsius at an initial moisture content of 1.80 %. The data presented in Table 3-2 show that there is no significant difference between the new and recycled potash. To avoid unnecessary waste of potash it was preferable to reuse potash that had been previously caked by completely drying and re-sieving the tested particles and these recycled particles were to be used in subsequent tests.

Table 3-2: Comparison of cake strength for new and recycled potash

Drying Method: Oven Drying at 40^{o}C Initial Moisture Content: 1.80 %		Drying Method: Air Drying Initial Moisture Content: 2.80%	
New Samples	Recycled Samples	New Samples	Recycled Samples
$\sigma_{mean} \pm U(\sigma_{mean})$	$\sigma_{mean} \pm U(\sigma_{mean})$	$\sigma_{mean} \pm U(\sigma_{mean})$	$\sigma_{mean} \pm U(\sigma_{mean})$
29.0 ± 3.1 KPa	26.3 ± 3.2 KPa	7.9 ± 1.4 KPa	9.2 ± 1.1 KPa

3.3.3 Cake strength measurements

3.3.3.1 Cake strength and initial moisture content

Figure 3-1 shows data and the relationship between initial moisture content and ultimate tensile stress of caked potash bed for oven drying and air drying with four different particle sizes. The calculated uncertainty bar for each test point and the best linear curve fit are also shown in the Figure 3-1. The error bars represent the 95% uncertainty limits at each particular initial moisture content using at least 12 sample caked rings calculated by equations (3-1), (3-2) and (3-3). The uncertainty, *U*, in Figure 3-1 was determined for the best straight line fit shown using only the data implied by the data points and their uncertainty. For both oven and air drying, these uncertainty values imply a relative uncertainty in the cake strength correlations of about 50% and 100% for d_{pm}=1.02 mm and 3.08 mm respectively when the initial moisture content is 1.8% (w/w). These experimental results, based on the potash samples with four different particle sizes, further confirmed the correlations obtained in Chapter two shown in Figure 2-14 that, for each drying method, there is a nearly linear relationship between the initial moisture content and cake strength. The best straight line fit in Figure 3-1 was selected as the best fit line that when through zero cake strength for the initial moisture content in the range 0.1 to 0.5% (w/w) as shown in Figure 2-14.

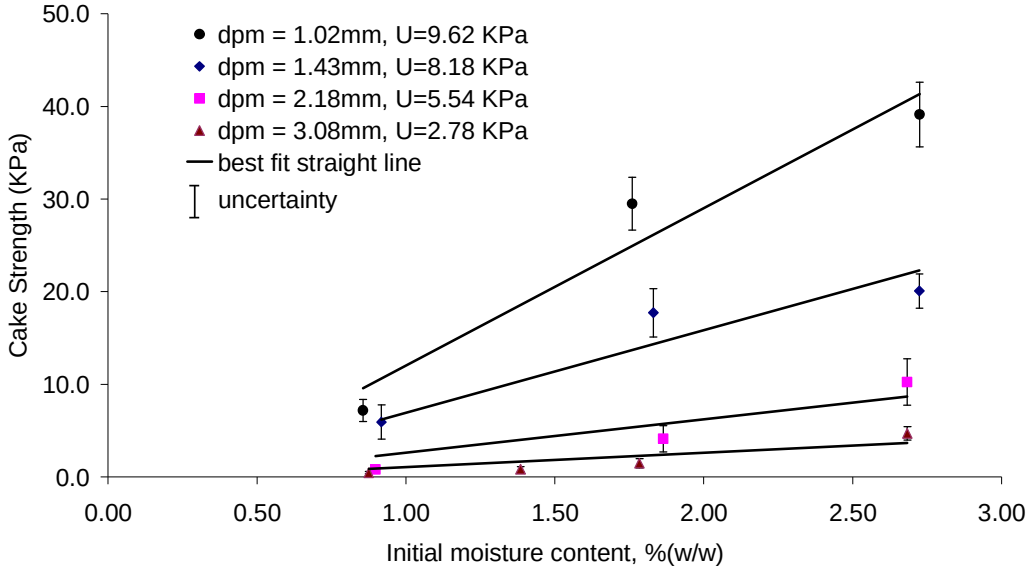

(a)

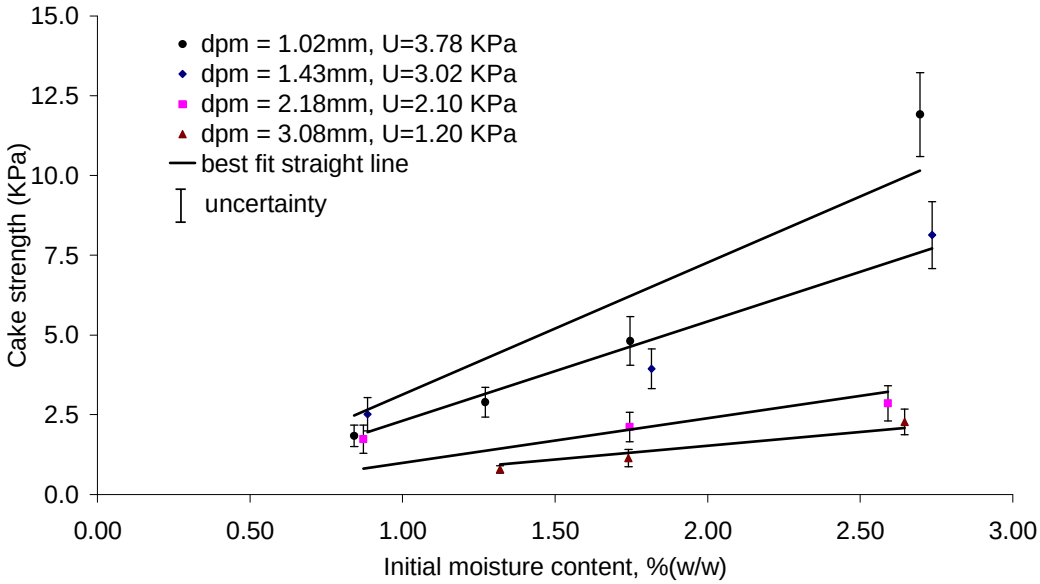

(b)

Figure 3-1: Potash cake strength versus initial moisture content for four different particle size ranges for (a) oven drying at 40^{o}C and (b) air drying at room conditions, $Mg \approx 0.02\%$.

3.3.3.2 Cake strength and particle size

To investigate the relationship between particle size and cake strength using the same drying method and initial moisture content, the cake strength was measured for four ranges of particle size. These data are plotted in Figure 3-2 for oven drying and with three different initial moisture contents. The 95% uncertainty bound for each test point, comprised of 15 or more tests, is indicated.

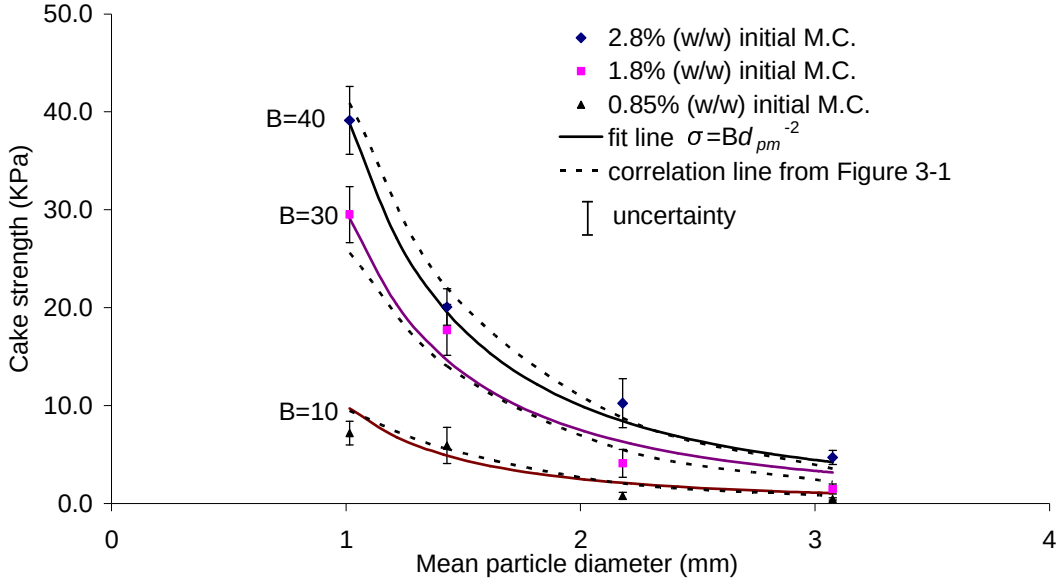

Figure 3-2: Cake strength versus average particle diameter for oven drying at 40ºC with three different initial moisture contents, Mg ≈ 0.02%

Figure 3-2 shows that the cake strength can be correlated approximately using an inverse square relationship with increasing particle diameter. The coefficient, *B*, of the $\sigma = Bd_{pm}^{-2}$ correlation decreases with increasing initial moisture content. It is known that caking process is caused by crystal bridges developing near the contact points between particles (Thompson, 1972, Kollmann and Tomas, 2001). As the number of

contact points per unit volume in a potash bed increase (i.e. the particle sizes decrease), it is expected that the cake strength will increase. If the number of contact points between particles is nearly constant for each particle, then with increasing particle diameter, the number of particle contact points per unit volume in each potash sample will decrease.

3.3.3.3 Cake Strength and Magnesium Concentration

Small concentrations of impurities, including carnallite and halite, are included during the production of potash (Arinze et al. 2000, 2001). The chemical composition, especially the content of magnesium, is expected to have a significant influence on cake strength. Tests were carried out to investigate the cake strength of a potash bed with variations in the content of magnesium. Three concentrations of magnesium were tested. To prepare these samples, a solution of magnesium chloride, $MgCl_2$ was added to the potash particles which were subsequently dried. In this case, the percentage Mg stands for mass fraction of the doped potash which is magnesium. Figure 3-3 shows the cake strength versus initial moisture content with three different concentrations of magnesium for oven and air drying. Using the same correlation procedure as Figure 3-1, the best fit straight lines for the linear relationship between cake strength versus initial moisture content are shown in Figure 3-3. These data show that as the concentration of magnesium in the potash increases, the cake strength increases significantly.

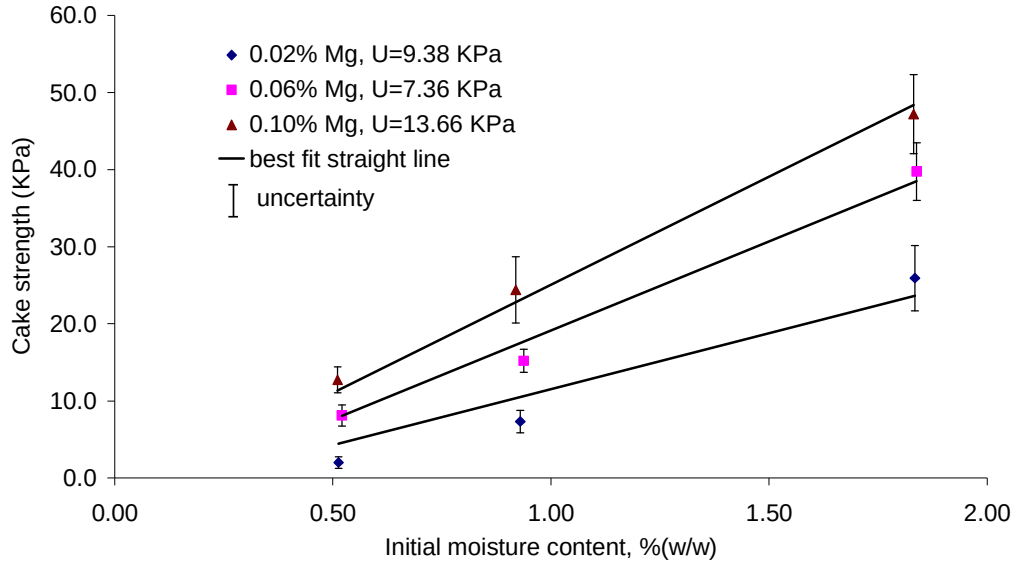

(a)

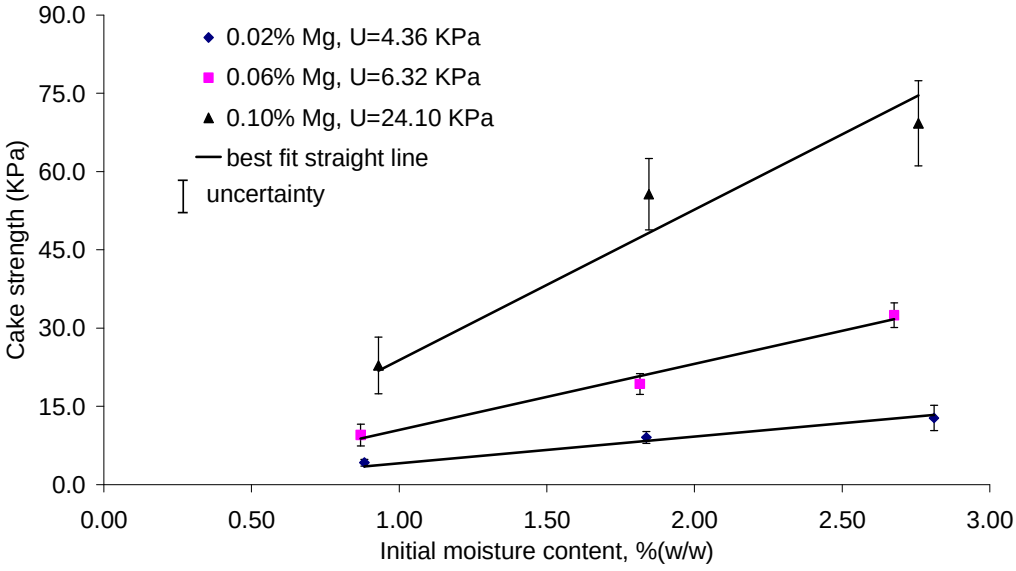

(b)

Figure 3-3: Potash cake strength versus initial moisture content with three different concentrations of magnesium for (a) oven drying at 40^{o}C and (b) air drying at room conditions, d_{pm} =1.02 mm

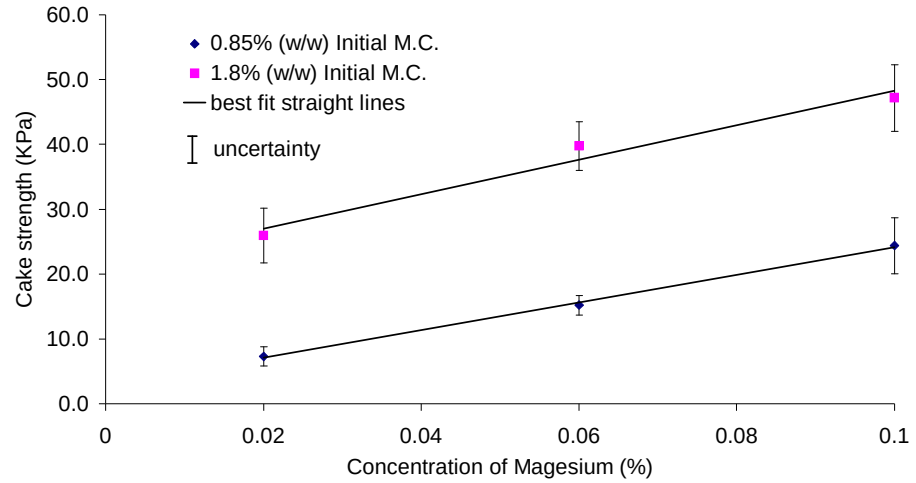

(a)

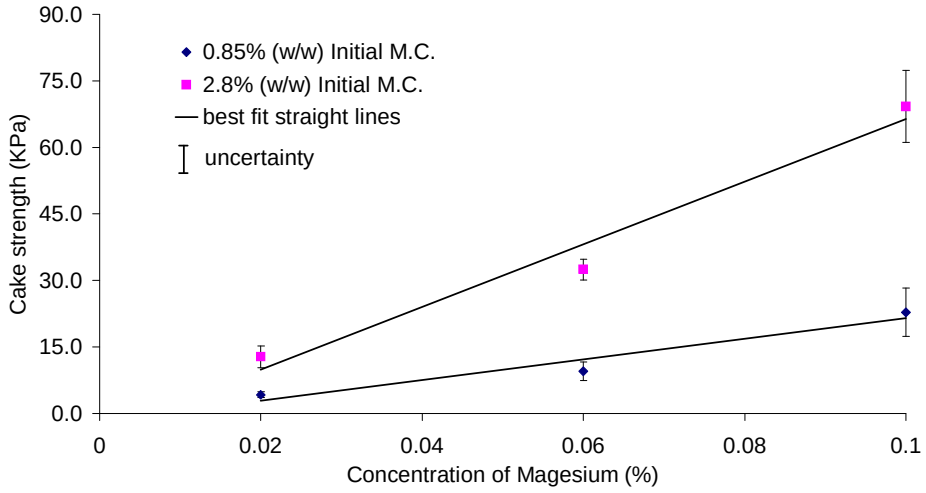

(b)

Figure 3-4: Potash cake strength versus concentration of magnesium for (a) oven drying and (b) air drying, d_{pm} =1.02 mm

Using the same data, the relationship between cake strength and concentration of magnesium is plotted in Figure 3-4 for each drying process. A linear relationship between cake strength and concentration of magnesium gives a reasonably good fit,

however, the intercept with the zero cake strength values imply negative magnesium content values for Figure 3-4 (a) but not (b). The reason for this difference is not clear.

It is found from the experimental results that the concentration of impurities such as magnesium or magnesium chloride salt, $MgCl_2$, in the salt solution of the liquid film on the potash particles alters the cake strength significantly. This impurity induces relative humidity at the air-liquid interface of potash particles from 85% for KCl to 52% $MgCl_2$ (Peng et al. 1999). It is expected that such a large decrease in the surface relative humidity would substantially decrease the liquid film evaporation rate when the interstitial bed air velocity is fixed or is constant and the ambient supply air humidity is constant. The relationships between cake strength and the content of magnesium shown in Figure 3-4 are consistent with the experimental data which predict that slower drying rates result in stronger cake strengths. Another reason for the change in cake strength may include the inclusion of attached water molecules in the $KMgCl_3 \cdot 6H_2O$ (carnallite) during recrystallization process. Further research should be conducted to explore why the content of magnesium has such a large impact on cake strength.

3.4 Conclusion and Summary

In this chapter, an experimental study has been carried out to determine the behavior of caked potash by measuring the cake strength using a centrifuge. The cake strength of potash was measured for tests in which the initial moisture content, particle size, magnesium content and drying time for each test were varied. For particle sizes ranging from 0.85 mm to 3.35 mm, new data confirms that the strength of caked potash increases essentially in a linear relationship with initial moisture content for each

method of drying. For other factors such as particle size and concentration of magnesium in potash, it was found that the cake strength of the bed will decrease with increasing particle size for the same initial moisture content and drying method. As well, it was also found that cake strength will increase essentially linearly with magnesium content for samples with the same initial moisture content, particle size and drying method.

Although more research on these factors, which influence the cake strength of potash, will increase this data base, producers of potash can use the data and correlations presented here to help minimize the impact of caked potash for storage and distribution in their bulk products.

CHAPTER 4

THEORETICAL/NUMERICAL MODEL OF RECRYSTALLIZATION NEAR A CONTACT POINT BETWEEN TWO POTASH PARTICLES

4.1 Introduction

A new centrifugal method to measure the cake strength of caked granular material with a known smaller uncertainty of measurement is developed in this thesis. The relationship between cake strength and the above variables is established using this accurate method, which can best represent the physical reality of caking behaviour for potash. It was found that cake strength increases linearly with initial moisture content, increases with the duration of drying for a particle bed (e.g. the cake strength more than doubled when the drying period was increased from 30 minutes to 10 hours), decreases with increasing particle sizes over the particle size range 0.85 mm to 3.35 mm, and increases with magnesium content (e.g. increased by a factor of three when the magnesium content was increased from 0.02% to 0.1%).

In this chapter, the recrystallization process due to thin film evaporation on wetted salt particles close to one contact point between two potash particles is theoretically formulated and numerically modelled. In next chapter, the recrystallization

process is simulated and the effects of the initial thickness of the liquid film electrolytic layer (i.e. initial moisture content), velocity of moving liquid film-air interface or rate of drying, and the degree of supersaturation on the solid surface near the contact point are considered. The simulated results are also compared to the achieved cake strength data in sample test beds of potash using the centrifugal method.

4.2 Background

Potash particles in bulk fertilizer products tend to have irregular shapes with sharp crystalline edges. The number of contact points between one particle and the surrounding particles will depend on the size distribution of particles in a bed and the packing of the bed (Chen et al. (2004)). For a well-packed bed of smooth particles, Chen and Tien (1973) have shown that there will be 6 to 12 contact points per particle. The geometry of each contact point will most likely be somewhat unique because as shown in Figure 1-2, each particle has a unique shape.

In this study we choose to avoid geometric complexity and concentrate on the effects of other important physical parameters such as the initial moisture content or film thickness, rate of evaporation or drying, and supersaturation effects on the surfaces near a typical contact point. Chen et al. (2004) also showed that for particle sizes equal to or less than 1 mm diameter the water content in a packed bed would remain macroscopically pendant or stationary for moisture contents less than 11% (w/w) - so the only mode of water transfer would be by gaseous diffusion and convection through the interstitial air.

Although it is not known, if any, what capillary motion will occur on particle surfaces near contact points during drying for this condition, each particle interstitial relative humidity in the bed will tend to cause an equal distribution of moisture content or film thickness on particle surfaces with the same chemical composition (Peng et al. 1999). That is, liquid film thickness are expected to be nearly uniform at each moisture content or film thickness during a drying process until the number of layers of water molecules on the surface become small. When potash particles experience a wetting process during storage, the water vapour from the air is adsorbed and accumulated on the surface of each particle and a saturated electrolytic solution layer is formed around each particle. This solution layer or liquid film will be saturated with solute ions from each salt at equilibrium conditions (Peng et al. 1999). During any subsequent drying process, there will be a redistribution of solute ions in the liquid film caused by water evaporation at the air-liquid film interface. This causes some supersaturation of solute at the liquid film-air interface and diffusion toward the solid crystal surfaces.

A two-dimensional schematic is presented near one contact point between two potash particles in Figure 4-1 which shows the two particles in contact at one point and the geometry of liquid film before drying. In this figure, one particle is shown as a flat surface and the other as a circular cone while a liquid solution layer is in contact with both particles near this contact point. As the liquid layer evaporates during a drying process, the liquid layer will get thinner throughout the entire liquid film and new KCl crystals will form on the solid surfaces where the ion concentration is at saturation or for slightly supersaturated conditions. When these new crystals are formed very close to contact point they have the potential to form bridges between particles. Even this

simplified geometry is more complex than necessary to study the recrystallization process and the physical effects. A simpler geometry with a uniform film thickness is shown in Figure 4-2.

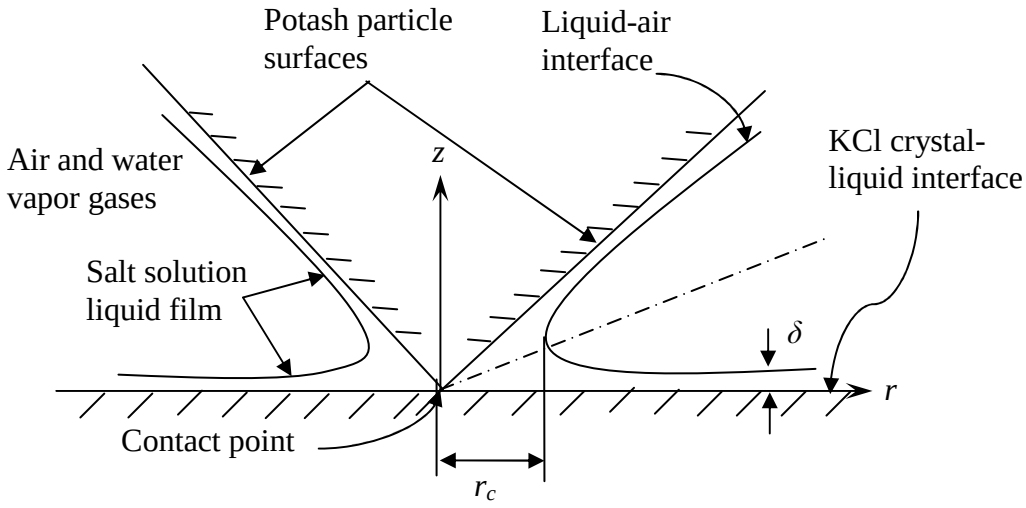

Figure 4-1: A two-dimensional axi-symmetric schematic for ion diffusion in a liquid film and recrystallization near a contact point between two potash particles

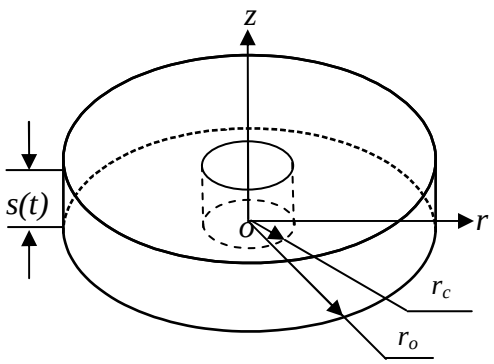

Figure 4-2: Schematic of aqueous salt solution of uniform thickness around a stretched contact point at $r = 0$

Figure 4-2 shows a liquid film of thickness, *s(t)*, which decreases as the film evaporates and where the fixed outer radius in this domain of interest near the contact point is r_o. On the boundary surfaces (z=*s(t)* and $0 < r < r_c$), and ($r=r_o$ and $0 \le z \le s(t)$), there is no mass diffusion. That is, the surface ($z = s(t), 0 < r < r_c$) has no evaporation which is taken to be the same as no mass transfer on the surface on the diagonal dashed line in the liquid film near the contact point in Figure 4-1 and the surface ($0 < z < s(t), r = r_o$) has no mass transfer because r_o/r_c is sufficiently large that the effects of the contact point are negligible. The line of symmetry ($0 < z < s(t), r = 0$) in Figure 4-2 has no mass transfer and it is transformed or mapped from the contact point in Figure 4-1. Elsewhere on the boundary, the top and bottom surfaces have two different mass transfers, on the top there is mass transfer due to the evaporation of water and on the bottom due to recrystallization of solute. Evaporation causes the domain in Figure 4-2 to decrease with time and recrystallization acts as a sink for the solute above the surface z=0. The value of r_c is chosen to have a value which is approximately equal to the initial film thickness very near the contact point r=0 (shown as r_c in Figure 4-1).

4.2.1 Diffusion in electrolytic solution

A comprehensive review of mass transfer in electrolytic solutions is given by Newman (1970). When a salt dissociates in solution, the ions move such that the net electric ion charge of the solution at any point remains near neutral. The movement of ions, which are driven by an electrochemical potential gradient (i.e. concentration gradient) in the absence of an external applied electrical potential difference, may be treated as pure diffusion process. In our case, the solution of a single KCl salt is

comprised of one cation (i.e. K^+) and anion (i.e. Cl^-) which is called a binary electrolyte. Since the requirement of zero electric current causes anions and cations to attract each other strongly and, ions of opposite charge will diffuse as pairs so a single salt will behave like one species. With no sources or sinks in the fluid media, the diffusion equation for a single electrolyte in a solution can be modeled by a differential equation for solute mass continuity at each point in the solution,

$$\frac{\partial c}{\partial t} = \nabla \cdot [D \nabla c] \tag{4-1}$$

where, c is the electrolyte concentration, units mole/m^3 or a dimensionless ratio when c is taken as a ratio which is the case used in this study where the reference concentration is for the saturation condition; D is the diffusion coefficient of the electrolyte, which is constant for a dilute solution at constant temperature, and is determined by (Newman, 1970).

$$D_o = \frac{D_+ D_- (z_+ - z_-)}{z_+ D_+ - z_- D_-} \tag{4-2}$$

where D_+ is diffusion coefficient for cation (for K^+ ion, $D_+ = 1.957 \times 10^{-9}$ m^2/s)

D_- is diffusion coefficient for anion (for Cl^- ion, $D_- = 2.032 \times 10^{-9}$ m^2/s)

z_+ is charge number for the cation (for K^+ ion, $z_+ = 1$)

z_- is charge number for the anion (for Cl^- ion, $z_- = -1$)

Using these data in equation (4-2), the calculated binary diffusion coefficient for KCl in a dilute solution is, $D_{KCl} = 1.994 \times 10^{-9} m^2 / s$.

It is known that potash also contains small amount of carnallite and halite (i.e. less than 2%). When moisture accumulates on potash particles, dissolution will occur when the ambient humidity exceeds a critical value (Peng at al. 1999). This aqueous solution film on particles surfaces will consist of three kinds of electrolyte i.e. KCl, NaCl and $MgCl_2$. A comparison of diffusion coefficients and solubility for these three salts is shown in Table 4-1.

Table 4-1: Values of diffusion coefficients of binary electrolytes in dilute solution and solubility in water at 25°C for KCl, NaCl, $MgCl_2$

Salt	Diffusion coefficient, D (m^2/s)	Solubility, c_s (g/100 g water)
KCl	1.99×10^{-9}	34.03
NaCl	1.61×10^{-9}	35.89
$MgCl_2$	1.25×10^{-9}	55.23

For a saturated solution Newman (1970) shows a decrease in D_{KCl} from the dilute solution value shown in Table 1 to about 1.77×10^{-9} m^2/s. When there are small changes in the solution temperature and concentration, c, throughout the domain of study, it can be shown that D will only change by a small amount. In this study temperature changes are expected to be less than 1°C and the solute concentration will be no greater than 40% of saturation conditions. At 40% supersaturation D_{KCl} will be about $1.37 \times 10^{-9} m^2/s$. It

will be shown later that this change in diffusion coefficient will not change the results significantly - so we can assume the diffusion coefficient is a constant equal to $1.77\times10^{-9}\,\mathrm{m}^2/\mathrm{s}$ for saturation conditions. This analysis of diffusion coefficient in a concentrated solution is equally applicable for the salts NaCl and $MgCl_2$. It is expected that the saturated salt solution diffusion coefficients of NaCl and $MgCl_2$ will be about 10% lower than the dilute solution value shown in Table 4-1. The remaining analysis is presented as it pertains to KCl only, but when these diffusion coefficients are nearly constant the results will be applicable to other salts.

Equation (4-1) governs the behaviour of the solute in the solution everywhere inside of a specified closed space or domain. A boundary condition must be specified on any component of the bounding surface of the domain shown in Figure 4-2. These boundary conditions are: the crystal solid surface on which there is mass deposition or recrystallization, the surfaces on which there is no mass flux, and the open evaporative surface which results in a moving boundary. It is noted that the evaporation of water from the exposed liquid film in Figure 4-2 does not result in loss of solute mass, however the concentration will change due to this evaporation. These are considered separately below.

4.2.2 Boundary conditions at crystal solid surface (*z*=0)

Theoretically, crystal growth can occur at any point at which $1 \le C$, however, when there is no nucleation site at a point, supersaturation conditions are required (i.e.1<*C*). Away from the salt crystal surfaces, nucleation sites are unlikely in thin films of liquid solution. Even on the crystal surfaces the solution may have to be in a

supersaturated state before crystallization occurs. Furthermore, the degree of supersaturation required for crystallization need not be uniform over the entire solid crystal surface in contact with the solution.

If the crystallization process on a crystal surface is entirely diffusion-controlled, the crystal growth rate is simply governed by the molecular diffusion equation at the interface (Mullin, 1993),

$$\bar{q} = D\nabla c \qquad (4\text{-}3)$$

where, $\bar{q}$ is mass flux of crystal growth on the surface.

Theoretically, the deposition of a new crystallization layer alters the position of the surface of the domain of solute in the solution by an amount equal to the thickness of the crystal in deposition layer. Since this deposition crystal layer is five times smaller than the corresponding drop in the liquid layer at $z=s$, it is neglected so that this problem, unlike the Stefan problem, is assumed to be linear and the surface $z=0$ remains flat. Before drying, the wetted potash particle is surrounded by a saturated KCl solution layer as shown near a contact point in Figure 4-1. During drying, the air-liquid interface is supersaturated due to water evaporation. This results in a concentration gradient between air-liquid interface and liquid-solid interface where the concentration is assumed to be at or near saturation. With evaporation, the supersaturated KCl salt ions diffuse from air-liquid interface towards to the solid surface as governed by Equation (4-1). This analysis does not include any buoyancy effects due to density variations and gravity interaction nor any coupling with heat transfer effects.

A typical average film thickness in a potash bed before drying can be estimated knowing the density of water, ρ_w, specific surface, $S_m(m^2/kg)$, initial moisture content, X, using the equation,

$$\delta = \frac{X}{\rho_w S_m} \tag{4-4}$$

For a potash bed for a particle size nearly 1 mm, the specific area, S_m, has been measured to be 1.55 m^2/kg (Zhou 2000) giving the initial film thickness, δ, between 6 and 60 μm for $0.01 \leq X \leq 0.1$ (i.e. initial moisture content 1% (w/w) and 10% (w/w)).

The thickness of a film of electrolytic solution on the particle surfaces in a potash bed will alter other properties such as effective thermal conductivity. For a small range of particle diameters, Yungwirth et al. (2006) showed that the effective thermal conductivity of potash will increase with moisture content such that there would be a 100% increase in effective thermal conductivity when the moisture content was increased from 0 to 2% (w/w) for $d_{pm} = 1.02$ mm. We might conclude from these data that increased surface moisture strongly increases the thermal contact between particles.

Chen and Tien (1973) suggested a range of 6-12 contact points for a particle within a typical particle bed comprised of nearly spherical particles. Potash particles, with an irregular crystalline shape, may have a slightly different number of contact points per particle in a packed bed. Using spherical particles the average distance between contact points on one particle can be estimated by equation,

$$d_o = \frac{d_{pm}}{\sqrt{2}} \tag{4-5}$$

where, d_{pm} is mean diameter of potash particle. This equation implies the average distance between contact points on a particle is between 10 and 100 times larger than the average film thickness for moisture contents between 10% (w/w) and 1% (w/w).

4.2.3 Boundary conditions at *z=s(t)*

The boundary condition on the air-liquid interface is now written for the exposed surface in Figure 4-2. Evaporation from an open surface is a moving boundary problem which needs to be solved in a time-dependent space domain (Crank 1984). The position of moving boundary has to be determined as a function of time and space. In this problem, the moving boundary at $z=s$ is assumed to have a constant speed, $u_s = ds/dt$, over the duration of the simulation and s is always positive.

In Figure 4-1, the point at $r=0$, $z=0$ is mapped into the line $r=0$, $0 \le z \le s$ in Figure 4-2. On this surface there is no mass flux. It is noted that this surface remains at the same level as the position of the surface from which there is evaporation. That is, the entire surface at $z=s$ is assumed to have a constant velocity, U_S. Since the boundary conditions at $z=0$ for $r>r_c$ and at $z=s$ for $r>r_c$ are uniform if r_o is chosen to be much larger than r_c there will be no mass flux at r_o except in the z direction. The value of r_c is only expected to change by a small fraction over most of the evaporation period. That is, the size of r_c is specified as a fixed fraction of the original liquid film thickness δ before evaporation starts (i.e. δ / r_c is $0.3 \le \delta / r_c \le 1.5$ for $0.2 \le S^* \le 1.0$). For $S^* < 0.2$ the value of r_c is expected to vary rapidly with time so the complete drying of the surface is not included in this study.

The boundary condition at *z=s(t)* needs special consideration. It is assumed that there is no mass transfer where $0 \le r \le r_c$ and $z = s$ in Figure 4-2. The interface between air and liquid where $r_c < r \le r_o$ and $z = s$, an infinitesimal layer (i.e very top layer or node in the finite difference formulation in the solution) is treated as a moving evaporation layer. Within this layer, the mass continuity of KCl salt is used as this moving boundary condition. It is assumed that the solution density is equal to solvent density, so the mass of KCl salt is calculated by multiplying solution concentration and solution volume. The moving boundary conditions for the evaporative surface area are given by,

$$\frac{\partial c}{\partial z}\Big|_{z=s(t)}(r,t) = 0 \qquad 0 \le r \le r_c \qquad (4\text{-}6)$$

$$\frac{d(c \cdot v_s)}{dt}\Big|_{z=s(t)} = 0 \qquad r_c < r \le r_o \qquad (4\text{-}7)$$

$$\frac{ds}{dt} = -u_s \qquad (4\text{-}8)$$

where, v_s is volume of infinitesimal evaporation layer or node region at $z = s$, m^3

u_s is constant moving boundary velocity, m/s.

Moving boundary problems have been reviewed by Crank (1984). One front-tracking method is used to solve the numerical model by varying the space grid size while keeping the number of grid points constant. The number of grid space intervals between a fixed boundary at *z*=0 and a moving boundary at *z*=*s* is kept constant and equal to *N*, so that the moving boundary always lies on the *N*th grid. Tracking a

particular grid line, the governing equation is transformed from constant space to moved grid points.

4.2.4 Problem formulation

The diffusion of a salt in a binary electrolytic solution governed by equation (4-1) for the axi-symmetric domain shown in Figure 4-3 is given using dimensionless cylindrical coordinates by,

$$\frac{\partial C}{\partial \tau} = \frac{1}{R}\frac{\partial}{\partial R}(R\frac{\partial C}{\partial R}) + \frac{\partial}{\partial Z}(\frac{\partial C}{\partial Z}), \quad 0 < Z \le S(\tau),\ 0 < R < R_o,\ \tau > 0 \qquad (4\text{-}9)$$

where $R = \frac{r}{r_c}, Z = \frac{z}{r_c}, S = \frac{s(t)}{r_c},\ C = \frac{c}{c_s},\ \tau = \frac{D \cdot t}{r_c^{\,2}}$.

The dimensionless boundary conditions are:

$$\frac{\partial C}{\partial R}\Big|_{R=R_o}(Z,\tau) = 0 \qquad R = R_o,\ 0 \le Z \le S(\tau) \qquad (4\text{-}10)$$

$$C\big|_{Z=0}(R,\tau) = C_a \qquad 0 \le R \le 1,\ Z=0 \qquad (4\text{-}11)$$

$$C\big|_{Z=0}(R,\tau) = C_b \qquad 1 < R \le R_o,\ Z=0 \qquad (4\text{-}12)$$

$$\frac{\partial C}{\partial Z}\Big|_{Z=S(\tau)}(R,\tau) = 0 \qquad 0 \le R \le 1,\ Z=S \qquad (4\text{-}13)$$

$$\frac{d(C \cdot V_S)}{d\tau}\Big|_{Z=S(\tau)} = 0 \qquad 1 < R \le R_o,\ Z=S \qquad (4\text{-}14)$$

where V_s is dimensionless volume of the evaporation layer for the node at $Z=S$

$$R_o = \frac{r_o}{r_c}$$

The dimensionless initial condition is:

$$\frac{dS}{d\tau} = -U_S = -\frac{u_s r_c}{D} \qquad (4\text{-}15)$$

which is constant for each simulation.

$$C\big|_{\tau=0}(Z,R) = 1 \qquad \tau=0,\ 0 \le R \le R_o, 0 \le z \le S_o \qquad (4\text{-}16)$$

which implies a saturation condition initially in the film, where $S\big|_{\tau=0} = S_o$, and $S_o = \frac{\delta}{r_c}$.

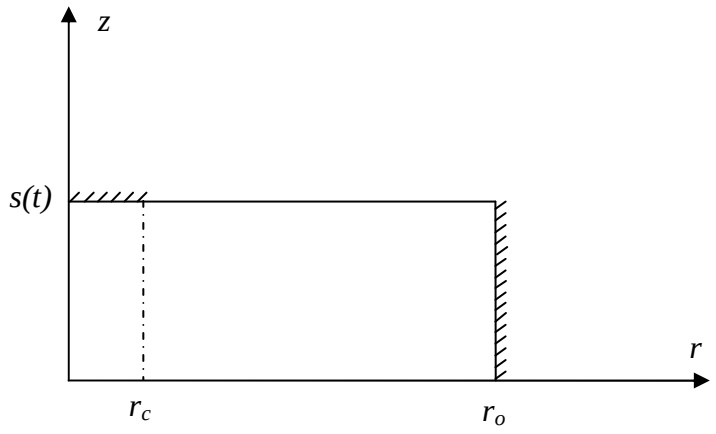

Figure 4-3: Schematic for the axi-symmetrical domain

4.2.5 Method of analysis

The variable space grid method described is used to solve the moving boundary problem. The number of space intervals, *N*, between fixed boundary *Z*=0 and moving boundary *Z=S(τ)* is chosen to be constant. Thus, the grid spacing is different at each time step such that the moving boundary is always on the *N*th grid line. By tracking a particular grid line, as opposed to constant Z, and differentiating with respect to time τ the following expression is obtained for *i*th grid line (Crank 1984),

$$\left(\frac{\partial C}{\partial \tau}\right)_i = \left(\frac{\partial C}{\partial Z}\right)_\tau \left(\frac{dZ}{d\tau}\right) + \left(\frac{\partial C}{\partial \tau}\right)_Z \qquad (4\text{-}17)$$

where $\frac{dZ}{d\tau} = \frac{Z_i}{S(\tau)}\frac{dS}{d\tau}$ and $\left(\frac{\partial C}{\partial \tau}\right)_Z$ is the term shown in Equation (4-9).

So the diffusion equation which is transformed from physical region to computational region of grid lines is given by,

$$\left(\frac{\partial C}{\partial \tau}\right)_i = \frac{1}{R}\frac{\partial}{\partial R}\left(R\frac{\partial C}{\partial R}\right) + \frac{\partial}{\partial Z}\left(\frac{\partial C}{\partial Z}\right) + \frac{Z}{S(\tau)}\frac{dS}{d\tau}\frac{\partial C}{\partial Z} \qquad (4\text{-}18)$$

An implicit numerical solution is used based on finite differences using the Taylor series expansion method. The alternating direction implicit (ADI) and Gauss successive iteration methods are used to solve discretized algebraic equations and moving boundary position *S(τ)* and grid size ΔZ are updated at each time step subject to the continuity of solute in the system.

Before each time step, the concentration of the very top grid line is determined first. The changed height for each time step due to water evaporation is applied to the very top finite volume in this model where the concentration is represented by the concentration at the top grids. The new concentration is determined by mass continuity of Equation (4-14). Then the grid size in the whole computational region is updated and Equation (4-18) is employed to solve diffusion process subject to other boundary conditions. In this model, the grid matrix is selected as 50×25 and the time step is 10^{-3} second. The selected tolerance used for the criteria of convergence with the numerical solution is 10^{-6}. The mass conservation for KCl inside the computational domain is determined for initial moisture content, X= 6% and evaporation rate, U_s=0.05 and shows that when the relative moving boundary position is S^*=0.2, the calculated mass of KCl including the deposition and the solute in the solution is 98% of the initial mass of KCl salt before drying.

4.3 Summary

A review of the literature revealed a need to analyze the caking process in particle beds if we are to correctly identify the most important physical factors that influence cake strength of a potash particle bed. This cake strength in a dried particle bed is assumed to be caused by crystal bridges forming between particles during the evaporative dying process which accompanies caking. In this chapter, a simplified diffusion model is presented to model the salt ion diffusion process and recrystallization near one geometrically simple contact point.

CHAPTER 5

SIMULATION OF NUMERICAL MODEL AND COMPARISON WITH EXPERIMENTAL DATA

In this chapter, numerical simulations of the model in Chapter 4 are used to determine the effects of changes for each independent parameter in this model such as: initial moisture content, rate of evaporation from the aqueous salt solution on the particle surface, relative size of the contact region compared to the initial film thickness of salt solution, and supersaturation properties on the solid crystal deposition surface near the contact point. Non-dimensional graphical curves of these simulations are used to compare the effects of each parameter for the deposition of salt crystals near the contact point. These results are compared to data for cake strength in potash specimens which were obtained for variation of initial moisture content, rate of drying and chemical composition of the particle surfaces. Also the numerical results considering the degree of supersaturation on the solid surface near the contact point are compared with the experimental results of surface roughness for NaCl and KCl after wetting and drying process investigated by Sun et al. (2006).

5.1 Dimensionless Terminology

In this model, the effects of the initial film thickness, δ, and the velocity of moving evaporation surface, $u_{s,}$ on the mass deposition distribution on the solid surface

of a particle are studied numerically. Results for mass deposition during the drying process are presented by varying the relative moving position, S^*, in consideration of two dimensionless parameters, U_S and S_o, which are given by equations (4-15) and (4-16) respectively. The relative moving position, S^*, is defined using the initial film thickness as,

$$S^* = \frac{s(t)}{\delta}. \qquad (5\text{-}1)$$

It is assumed that the evaporation rate depends only on the selected value of U_S, and the thickness of contact region, r_c, is constant so S_o is only function of initial moisture content, X. The numerical model is used to explore the impact of the evaporation rate and initial moisture content on recrystallization of potash particles. For each independent factor considered, the local distribution of mass deposition on the particle surface， the total deposition inside the contact region during the drying process, the deposition per unit area inside of contact region during drying process and the deposition per unit area at $r=r_o$ during the drying process are plotted in dimensionless forms. These are shown in Figures 5-1 to 5-8.

The mass of deposition of KCl crystals on a potash particle surface between two radii, r_1 and r_2, during drying process is determined by,

$$m = \int_0^t \int_{r_1}^{r_2} D \left.\frac{\partial c}{\partial z}\right|_{z=0} 2\pi r dr dt \qquad (5\text{-}2)$$

Two dimensionless mass distributions are used in Figures 5-1 to 5-8 to make the results more general. These are defined using the following terms:

$$M_c = \frac{m_c}{m_{ci}} \tag{5-3}$$

where, M_c is the total dimensionless mass fraction of crystal deposition inside the contact region; m_c is the total crystal mass deposition inside contact region; m_{ci} is the initial mass of KCl salt in the liquid film inside the contact region.

$$N_c = \frac{n_c}{n_i} \tag{5-4}$$

where, N_c is dimensionless mass fraction of crystal deposition per unit area inside the contact region; n_c is the average crystal mass deposition per unit area inside the contact region; n_i is the initial mass of KCl salt per unit area in the thin film solution.

N_o can be used to characterize the mass fraction at $r=r_o$ using

$$N_o = \frac{n_o}{n_i} \tag{5-5}$$

where, N_o is dimensionless mass fraction of crystal deposition per unit area at $r = r_o$; n_o is the crystal mass deposition per unit area at $r = r_o$.

N can be used to characterize the mass fraction at any radius r

$$N = \frac{n}{n_i} \tag{5-6}$$

where, N is dimensionless mass fraction of crystal deposition per unit area; n is the crystal mass deposition per unit area at r.

5.2 Numerical Results

5.2.1 Simulation with a range of initial moisture contents

The effect of initial film thickness on particle surface before drying was investigated in this model. A range of initial moisture contents from 2% (w/w) to 7% (w/w) were selected and the corresponding dimensionless initial positions of moving evaporation surface, S_o, are from 0.4 to 1.3. The dimensionless mass depositions of KCl inside of contact region, M_c and N_c, are plotted in Figures 5-1 and 5-2.

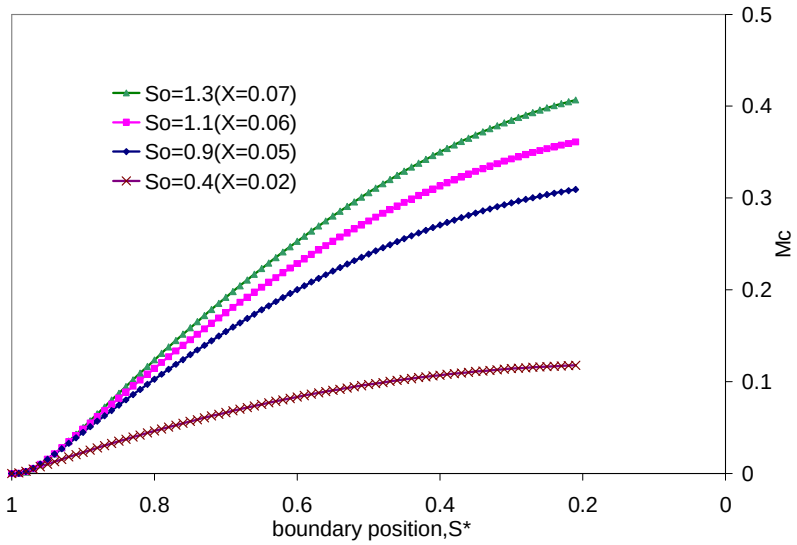

Figure 5-1: Dimensionless crystal mass deposition inside contact region, M_c, versus dimensionless moving boundary position, S^*, with different initial film thicknesses, S_o (initial moisture content, X), as a parameter, U_S=0.05, $C_a = C_b = 1.0$

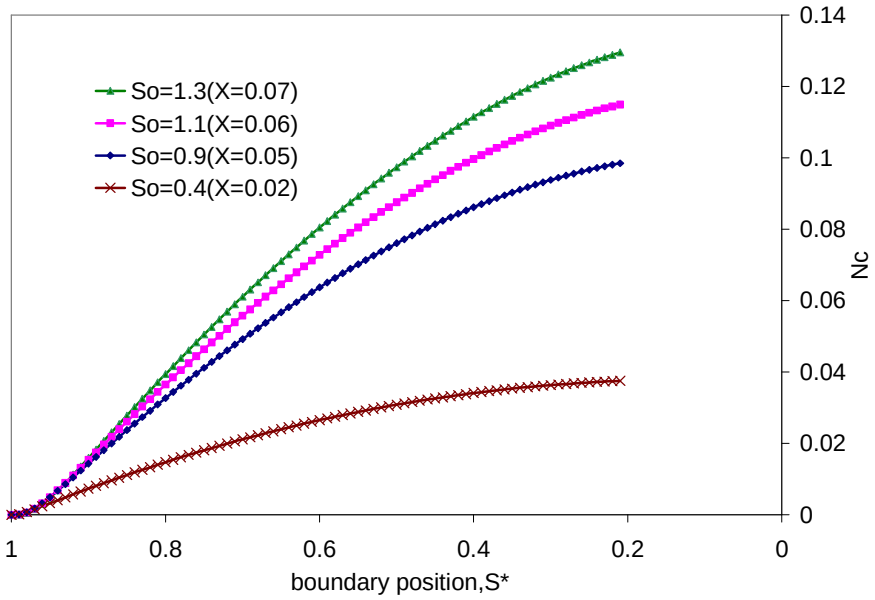

Figure 5-2: Dimensionless crystal mass deposition per unit area inside contact region, N_c, versus dimensionless moving boundary position, S^*, with different film thickness, S_o (initial moisture content, X), as a parameter, U_S=0.05, $C_a = C_b = 1.0$

It is shown in Figures 5-1 and Figure 5-2 that the mass deposition of KCl crystals inside contact region significantly increases with greater initial moisture content where S^*=1 corresponds to the initial position of the liquid film and S^*=0.2 corresponds to the time when 80% of the film has evaporated. Figure 5-3 shows the local distribution of dimensionless mass crystal deposition per unit area. It is shown that, as the initial film thickness is increased, the mass deposition in the contact region ($0 \le r \le r_c$) will increase.

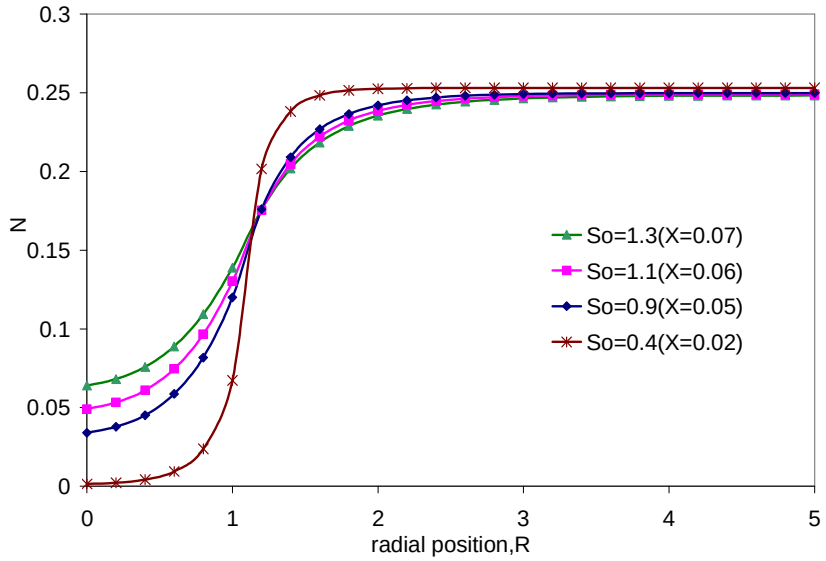

Figure 5-3: Local distribution of crystal mass deposition per unit area, N, versus radial position, R, with different initial film thicknesses, S_o (initial moisture content, X), as a parameter, U_S=0.05， S^*=0.2, $C_a = C_b = 1.0$

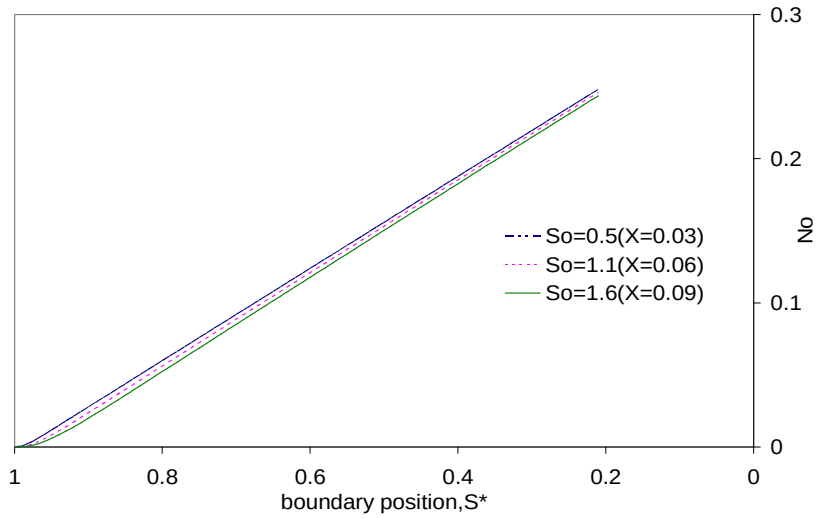

Figure 5-4: Dimensionless crystal mass deposition per unit area at $r=r_o$, N_o, versus dimensionless moving boundary position, S^*, with different initial film thicknesses, S_o (initial moisture content, X), as a parameter, U_S=0.05, $C_a = C_b = 1.0$

Figure 5-4 shows that the crystal mass deposition on the region far away from contact point which decreases slightly with initial moisture content because the thicker initial film needs more time to reach a quasi-steady state.

5.2.2 Simulation with a range of evaporation rates

The crystal mass depositions inside contact region with a range of evaporation rate (i.e. dimensionless moving surface velocity) from 0.005 to 0.5 are plotted in Figures 5-5 and 5-6.

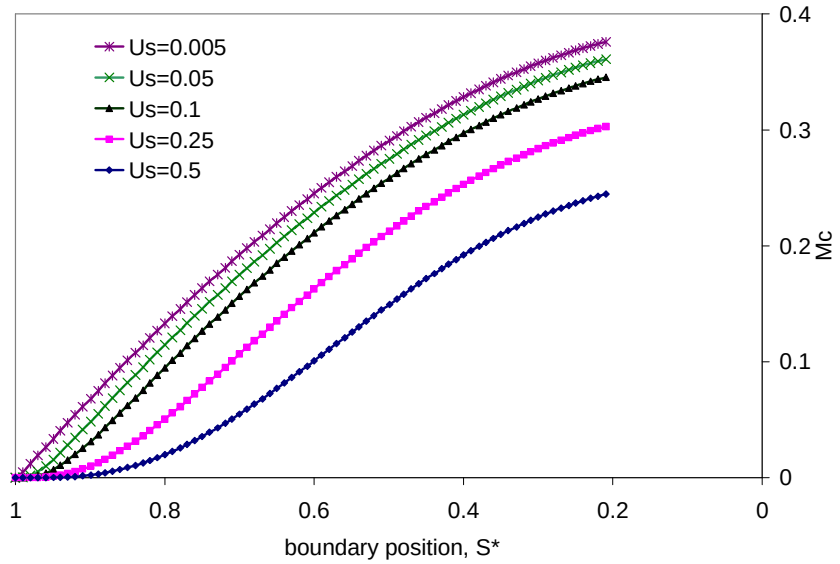

Figure 5-5: Dimensionless crystal mass deposition inside contact region, M_c, versus dimensionless moving boundary position, S^*, with different moving boundary velocities, U_S, as a parameter, S_o=1.1(X=0.06), $C_a = C_b = 1.0$

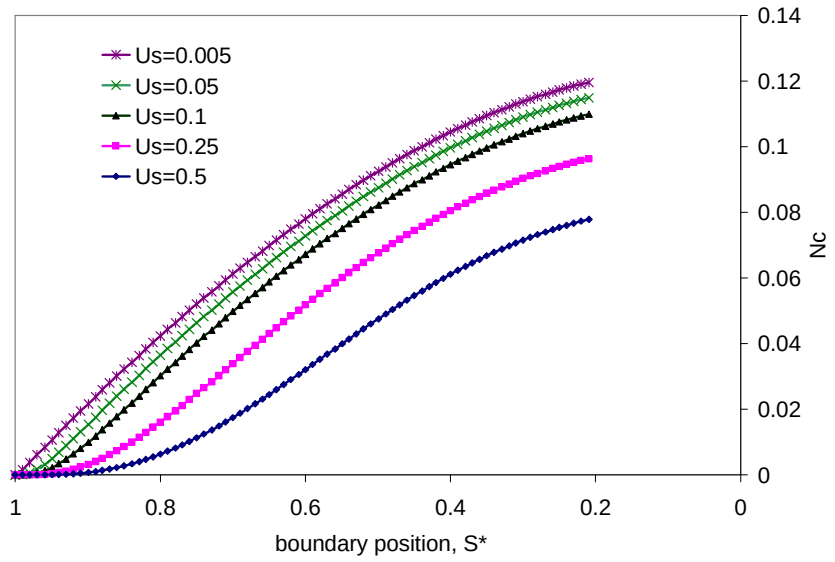

Figure 5-6: Dimensionless crystal mass deposition per unit area inside contact region, N_c, versus dimensionless moving boundary position, S^*, with different moving boundary velocities, U_S, as a parameter, S_o=1.1(X=0.06), $C_a = C_b = 1.0$

It is shown in Figure 5-5 and Figure 5-6 that the mass deposition of KCl crystals inside contact region increases with slower evaporation rates (i.e moving boundary velocity U_S). With 6% initial moisture content, the total drying time when S^*=0.2 corresponding to the Us=0.05 is 11 seconds and 1.1 seconds for Us=0.5. It will be shown later that the supersaturation in the film of solution increases with faster evaporation rate.

It will be shown later that the supersaturation in the film of solution increases with faster evaporation rates. This results in more mass of solute in the solution and less mass of crystal deposition distributed on the particle surface at the same S^*. This is shown in Figures 5-7 and 5-8. As the moving boundary velocity is decreased, the mass deposition will increase everywhere.

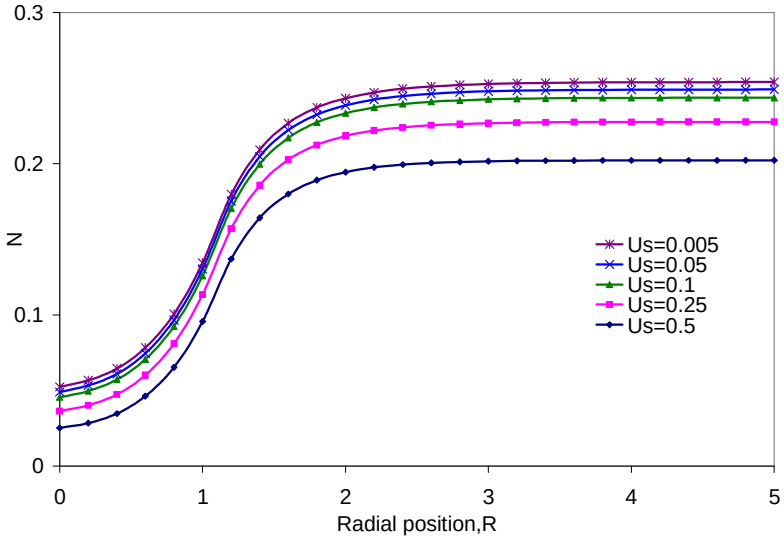

Figure 5-7: Local distribution of crystal mass deposition per unit area, N, versus radial position, R, with different moving boundary velocities, U_S, as a parameter, S_o=1.1(X=0.06), S^*=0.2, $C_a = C_b = 1.0$

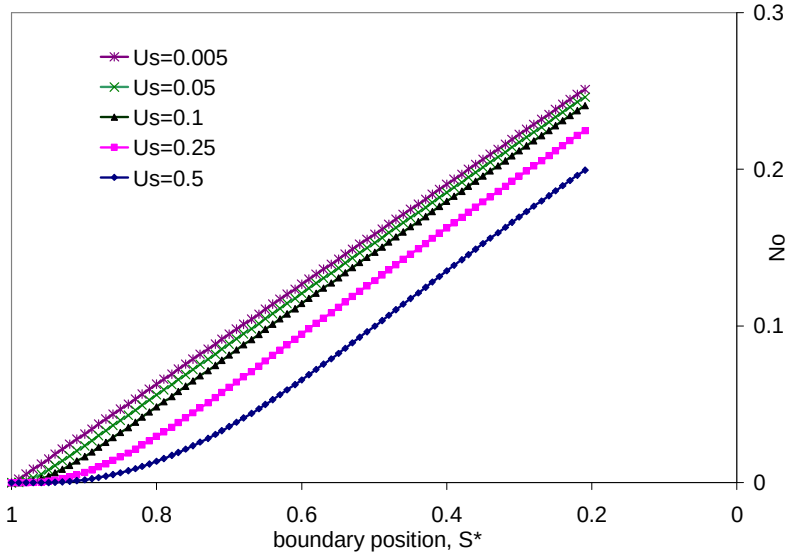

Figure 5-8: Dimensionless crystal mass deposition per unit area at $r=r_o$, N_o, versus dimensionless moving boundary position, S^*, with different moving boundary velocities, U_S, as a parameter, S_o=1.1(X=0.06), $C_a = C_b = 1.0$

5.2.3 Simulation with a range of supersaturation on particle surface

Another factor considered in this model is supersaturated concentrations on the crystal growth surface. Mullin (1993) showed that crystals tend to grow primarily at nucleation sites on surfaces. He also showed that very small crystals can have a solubility significantly higher than those of macrocrystals. Variations in supersaturation can be investigated using this symmetric model near one contact point with the surface of contact region, $0 \le R \le 1$, at saturation conditions while the exterior region crystal surface is supersaturated. In Figure 5-9, 5-10, 5-11 and 5-12 we use the numerical model to simulate results using the following boundary conditions,

$$C\big|_{Z=0}(R,\tau) = C_a = 1 \qquad 0 \le R \le 1,\ \text{Z=0} \qquad (5\text{-}7)$$

$$C\big|_{Z=0}(R,\tau) = C_b \qquad 1 < R \le R_o,\ \text{Z=0} \qquad (5\text{-}8)$$

where, C_b is a dimensionless supersaturated concentration parameter.

Supersaturation is shown to be very sensitive to a few percent increases in supersaturation for C_b (i.e. the mass accumulation in the contact region in Figure 5-9 and 5-10 increases by a factor of 5 or more as C_b is changed from 1.00 to 1.04). The reason for this increase is made clear from Figure 5-11 and 5-12 which show that the change in deposition per unit area at R_o is quite small; but, inside the region $1<R<2$ and including the contact region, $0 \le R \le 1$, the mass deposition per unit area is strongly affected. Figure 5-12 shows mass deposition decreased for $1<R<2$ and increased for $0 \le R \le 1$. The negative values for N imply that mass is removed (i.e. crystal dissolution) which is subsequently deposited in the raised N value regions.

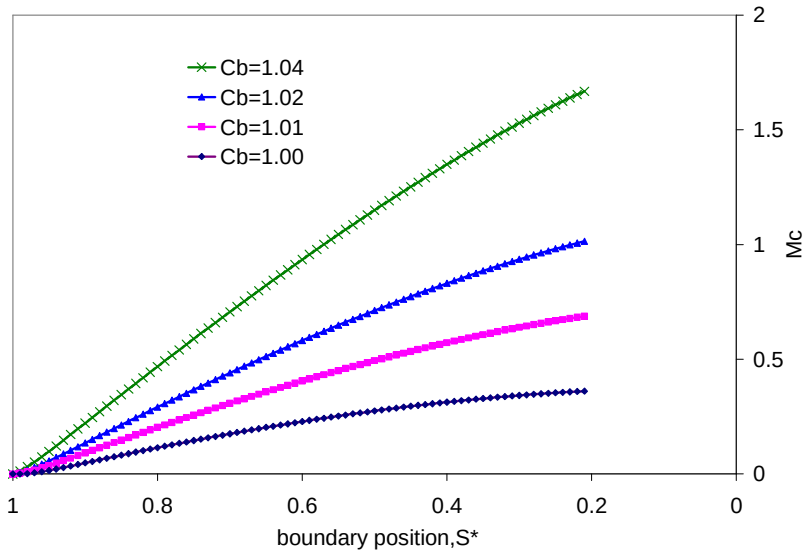

Figure 5-9: Dimensionless crystal mass deposition inside contact region, M_c, versus dimensionless moving boundary position, S^*, with C_a=1.0 and saturated and supersaturated boundary conditions, Us=0.05 and S_o=1.1

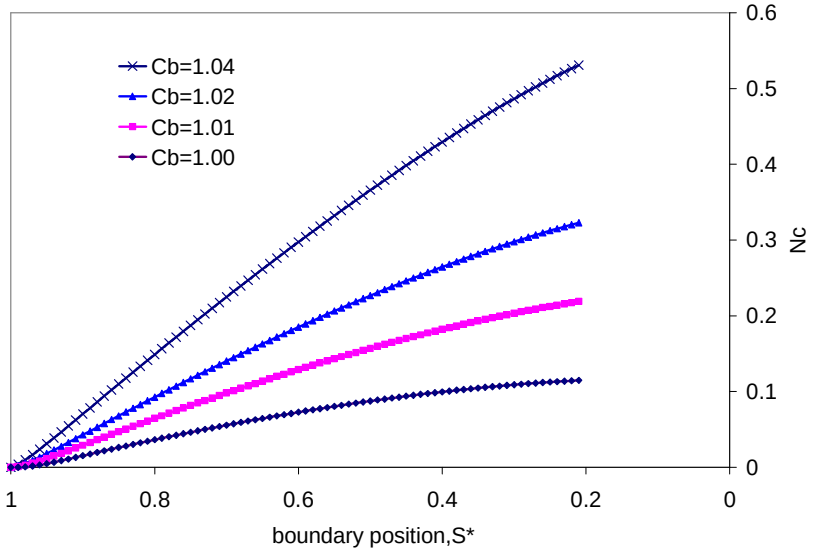

Figure 5-10: Dimensionless crystal mass deposition per unit area inside contact region, N_c, versus dimensionless moving boundary position, S^*, with C_a=1.0 and saturated and supersaturated boundary conditions, Us=0.05 and S_o=1.1

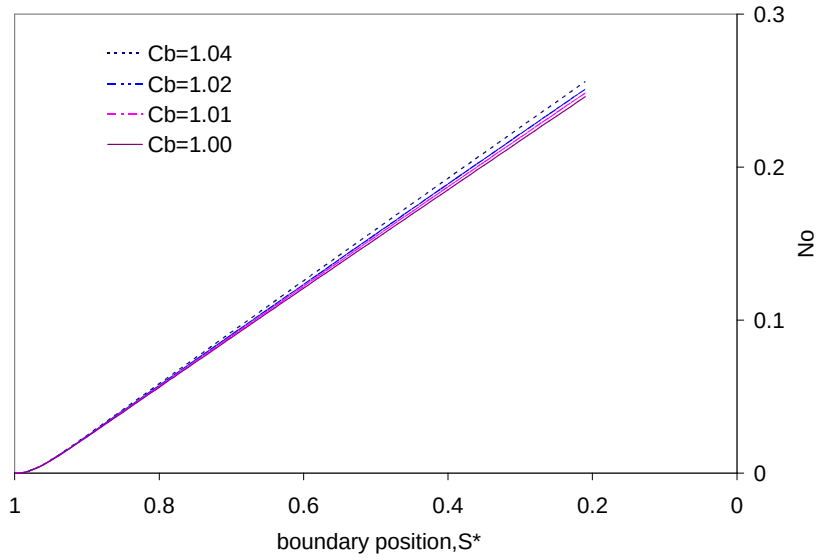

Figure 5-11: Dimensionless crystal mass deposition per unit area at R_o, N_c, versus dimensionless moving boundary position, S^*, with C_a=1.0 and saturated and supersaturated boundary conditions, Us=0.05 and S_o=1.1

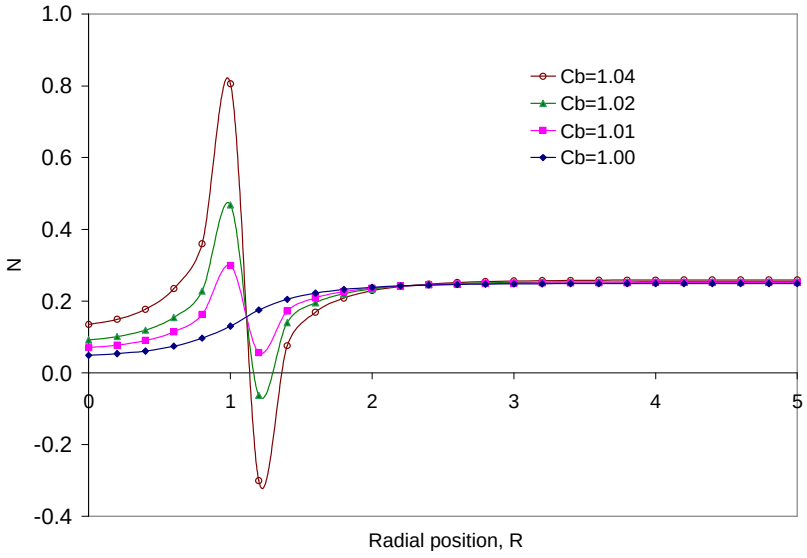

Figure 5-12: Local distribution of crystal mass deposition per unit area versus radial position, R, with C_a=1.0 and saturated and supersaturated boundary conditions, Us=0.05, S_o=1.1 and S^*=0.2

5.3 Analysis and Discussion

5.3.1 Mass deposition and cake strength

The relationship between mass deposition, M_c, in the contact area and initial moisture content, X, with moving boundary velocity, Us, as the parameter and the relationship between M_c and Us with X as the parameter are plotted in Figure 5-13 and Figure 5-15 using the same numerical results shown in Figure 5-1 and Figure 5-5.

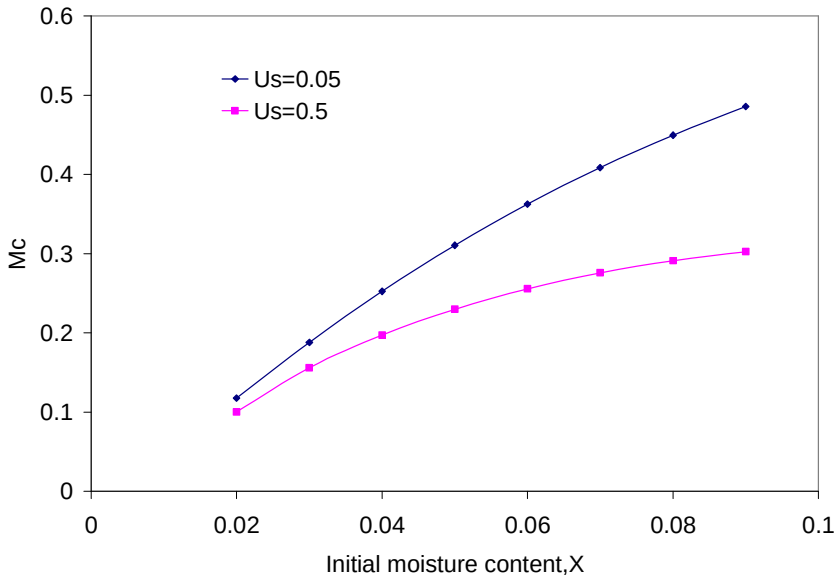

Figure 5-13: Dimensionless crystal mass deposition inside contact region, M_c, at S^*=0.2 versus initial moisture content, X, and U_S as a parameter, $C_a = C_b = 1.0$

The simulated results in Figure 5-13 show that, if the initial moisture content is increased from 3 to 4% (w/w) for the same drying rate and other boundary conditions, the mass deposition in the contact area will increase by a factor of 1.3. This result is consistent with the experimental cake strength data which showed that the cake strength

of a bed of potash particles increased by a factor 1.3 to 1.5 when the initial moisture content was increased from 3 to 4% (w/w) for the same drying process. Table 5-1 shows a comparison of these experimental data for cake strength and numerical results in crystal mass deposition inside contact region between two potash particles for two different drying processes and two different initial moisture contents. The selected surface velocities for these numerical simulations (i.e. $u_s = 2.8\,\mu\text{m/s}$ and $u_s = 28\,\mu\text{m/s}$) are approximately consistent with the oven drying and air drying data.

Table 5-1: Comparisons between experimental cake strength data after both oven drying and air drying and simulations for crystal mass deposition inside contact region between two potash particles for evaporation rate, d_{pm}=1.02 mm

Experimental Data (oven drying)		Numerical Results (*Us*=0.05)	
X (w/w *%)*	Cake strength(KPa)	*X*(w/w *%)*	M_c (*S**=0.2)
1.8	29	2	0.12
2.8	39	3	0.19
3.7	57	4	0.25
Experimental Data (air drying)		Numerical Results (*Us*=0.5)	
X (w/w *%)*	Cake strength(KPa)	*X* (w/w *%)*	M_c (*S**=0.2)
1.7	5	2	0.10
2.8	12	3	0.15
3.7	16	4	0.20

The same data shown in the Table 5-1 are plotted in Figure 5-14 to compare the numerical results at U_S=0.05 and U_S=0.5 with experimental data for oven drying and air drying respectively.

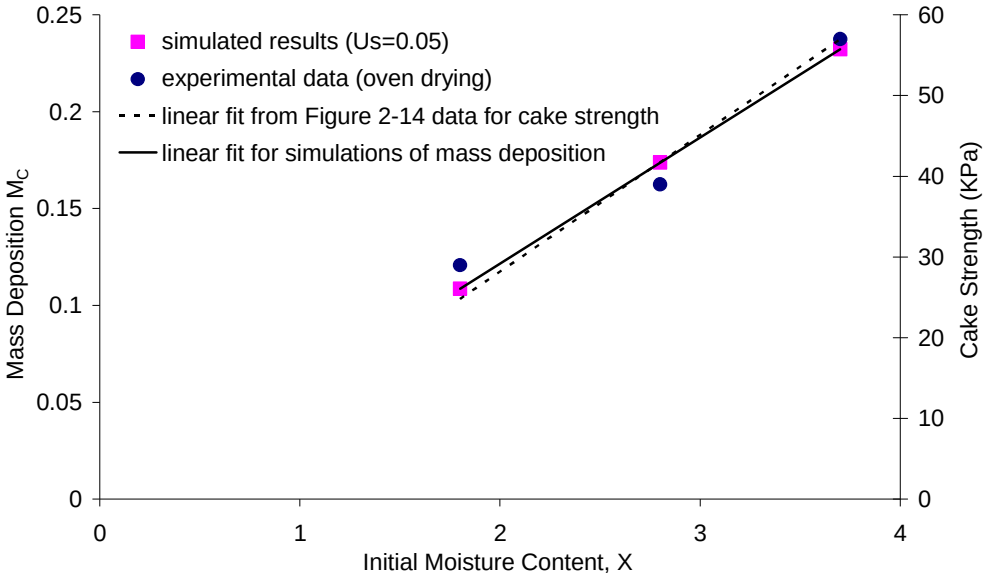

(a)

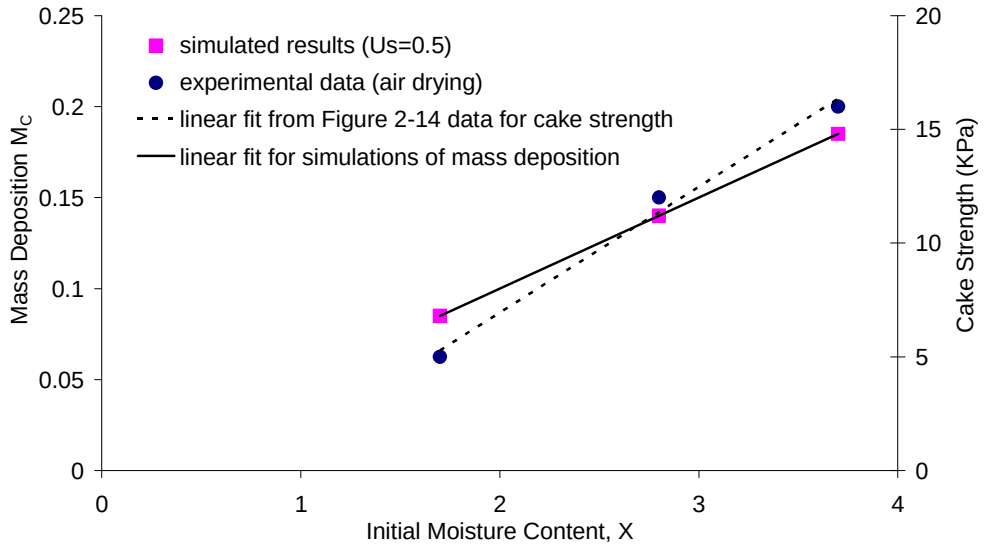

(b)

Figure 5-14: Comparison of numerical results of crystal mass deposition inside contact region and experimental data of cake strength for (a) U_S=0.05 and oven drying (b) U_S=0.5 and air drying, d_{pm}=1.02 mm

It is shown that both numerical results for crystal mass deposition inside contact region and experimental data for cake strength both fit a linear relationship with increasing initial moisture content. The comparison shown in Figure 5-14 implies a one-to-one relationship between simulated crystal mass accumulation results and measured experimental cake strength data; however, there can be other factors such as magnesium content and external pressure stresses that could alter the cake strength.

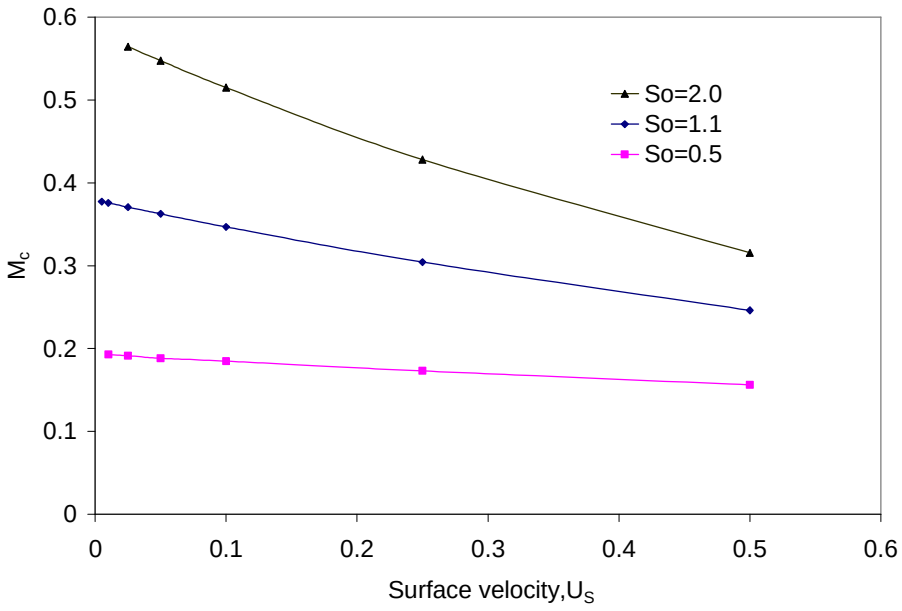

Figure 5-15: Dimensionless crystal mass deposition inside contact region, M_c, at S^*=0.2 versus moving boundary velocity, U_S, and S_o as a parameter, $C_a = C_b = 1.0$

Figure 5-15 show that the depositions of KCl crystals inside contact region increase with slower evaporation rate. Conversely the cake strength decreases with increased evaporation rate. This numerical result in Figure 5-15 which shows a one third decrease in mass deposition in the contact region when the evaporation rate was increased by a factor of 10 from 0.05 to 0.5 is consistent with the experimental data for

cake strength which showed that, when the drying speed was increased by a factor of about 25 for the same initial moisture content, the cake strength was one half. These comparisons of two somewhat different things, mass deposition and cake strength, implies a direct relationship between mass deposition of crystals near a typical contact point between particles in a caked bed and the cake strength of the bed. That is, we have no directly measured data on the mass deposition due to recrystallization - so we have made comparisons with the one quantity that we have directly measured, cake strength. Future experiments will be required to better establish the validity of this relationship over a wide range of properties and test conditions. As well, more sophisticated experiments would be needed to directly relate crystal bridging near contact points and the evaporation of water from thin films.

Another important factor in the caking process is the concentration of impurities such as magnesium or magnesium chloride salt $MgCl_2$ in the salt solution of the liquid film on the potash particles. This impurity reduces the water vapour induced relative humidity at the air-liquid interface from 85% for KCl to 52% $MgCl_2$ (Peng et al. 1999). Such a large decrease in the surface relative humidity would substantially decrease the liquid film evaporation rate when the interstitial bed air velocity is fixed or is constant and the ambient supply air humidity is constant. Experimental data for cake strength showed that increasing the surface magnesium content from 0.02% to 0.1% resulted in a three fold increase in cake strength when the same method of drying was used for testing samples. These simulation results for the effect of film surface speed are also consistent with these experimental data.

Zhou (2000) measured the apparent thermal conductivity of granular potash using a steady state method. It was shown that there was a 20% increase in the apparent thermal conductivity between dry and re-dried samples, which indicates that re-drying creates caking bridges between potash particles which decrease the contact resistance between particles and enhances heat conduction between the particles. These experimental results are consistent with the experimental data for cake strength and with the simulation results using this model.

5.3.2 Thickness of deposited crystal layer and roughness

The results in Figure 5-12 can be used to predict the thickness of the recrystallization layer shown in Figure 5-16.

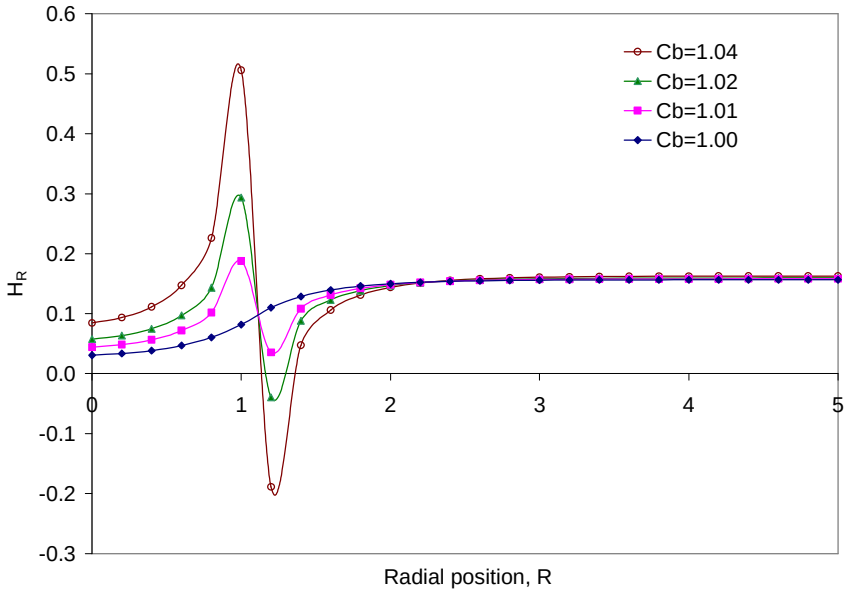

Figure 5-16: Local distribution of height of deposited crystal layer on potash particle surface versus radial position, *R*, with C_a=1.0 and saturated and supersaturated boundary conditions, *Us*=0.05, S_o=1.1 and *S**=0.2

This figure implies another interesting prediction-crystal surfaces on particles which are initially smooth can, due to non-uniform variations in the supersaturation boundary conditions on these solid surfaces, become rough during a recrystallization process. That is, the uneven mass deposition for the contact region shown in Figure 5-12 and Figure 5-16 will not only enhance the likehood of crystal bridging between particles but the surface will be rougher after recrystallization compared to the original surface which was assumed to be smooth.

In Figure 5-16, the dimensionless height of deposited crystal layer on potash particle surface, H_R, is defined as $H_R = n/(\rho_{KCl}\delta)$ where ρ_{KCl} is the density of pure solid KCl crystal. For example, the recrystallization layer thickness at R = 5 would be 6.3 μm for these conditions when the initial film thickness, δ, is 38.7 μm for an initial moisture content of 6% (w/w) for particles with $d_{pm} = 1.015$ mm. In the contact region, R=1, the peak crystal height would be 11.4 μm for C_b=1.02 and 19.6μm for C_b=1.04, implying that too high a value of C_b (i.e. C_b>1.02) can lead to a somewhat unrealistic result that the peak deposition height would approach the original liquid film height. This prediction of increased roughness after drying is consistent with the finding of Sun et al. (2006) who showed that NaCl and KCl crystal surfaces, with less than 1% impurities and cut with a diamond cutter with a low initial roughness before wetting became about five times rougher after drying. Furthermore, this measured roughness was distributed over the entire cut surface, suggesting that the crystal surfaces can have significant variations in the degree of saturation due to slight chemical potential changes at the liquid-solid interface. In a particle bed, there is no apparent reason that the contact points between one particle and the surrounding particles would be the site of an

enhanced deposition surface as implied in Figure 5-12 and Figure 5-16. Such contact points may have an equal probability of reduced deposition or even mass removal from the surface after drying. If this were the case, some contact points between particles may enhance the caking process, as implied by Figure 5-12 and Figure 5-16 while others would have a reduced probability of caking. This observation may be one of many reasons why various samples of wetted and dried particle beds show significant variations in the measured cake strength even when every effort is made to have identical test conditions.

5.3.3 Supersaturation and changes in the diffusion coefficient

As stated by Newman (1970), the diffusion coefficient of concentrated solution such as saturated or supersaturated KCl salt solution is a function of ion concentration of the electrolyte solution. In this research, the ion concentration distribution on the evaporation surface during drying is shown in Figures 5-17 and 5-18.

Figure 5-17 shows that the ion concentration on the evaporation surface increases with increasing evaporation rate. It is also shown in Figure 5-18 that the ion concentration increases with initial moisture content and the film boundary position corresponding to the peak value of ion concentration decreases with initial moisture content. These figures imply that ion concentration on the moving boundary may be more sensitive to evaporation rate than the initial moisture content. For example, when evaporation rate, Us=0.5 at initial moisture content X=6% (w/w), the ion concentration will increase to a maximum value of 40% supersaturation when moving boundary position, S^*, is about 0.6.

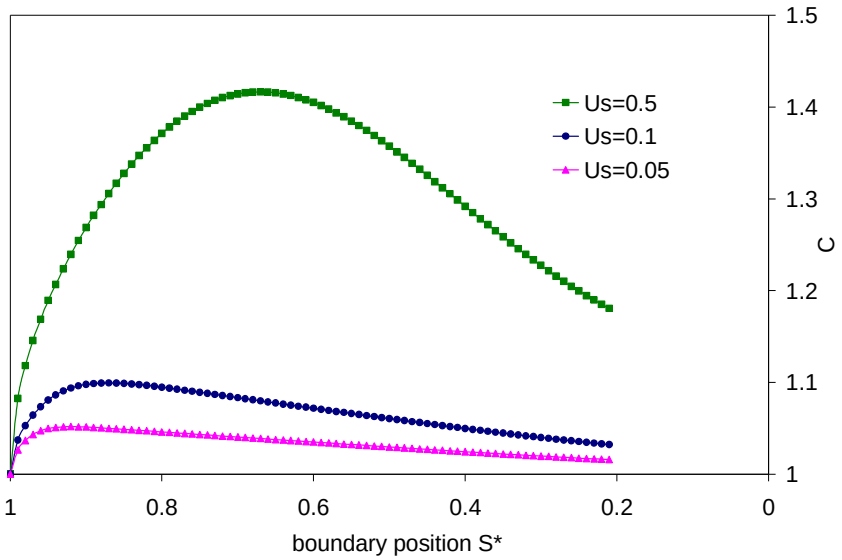

Figure 5-17: Dimensionless ion concentration, C, on the moving evaporation surface (i.e.$Z=S(\tau)$) versus dimensionless moving boundary position, S^*, U_S as a parameter, S_o =1.1(X=6%, $R=R_o$), $C_a = C_b = 1.0$

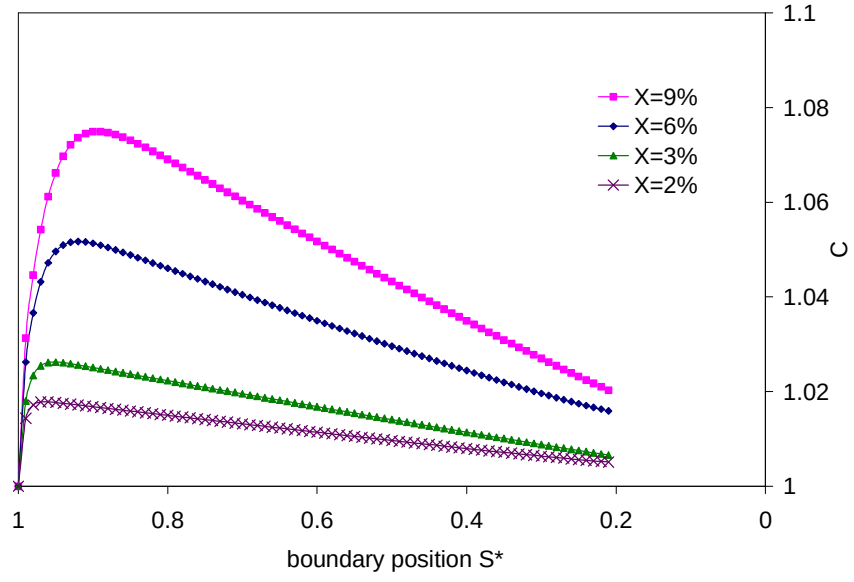

Figure 5-18: Dimensionless ion concentration, C, on the moving evaporation surface (i.e.$Z=S(\tau)$, $R=R_o$) versus dimensionless moving boundary position, S^*, X as a parameter, U_S=0.05, $C_a = C_b = 1.0$

A sensitivity study of variations in diffusion coefficient caused by supersaturation is shown in Figure 5-19. This figure suggests that the peak 40% supersaturation shown in Figure 5-17 for *Us*=0.5, which would cause a about 20% decrease in the diffusion coefficient, would not alter the previously shown results significantly.

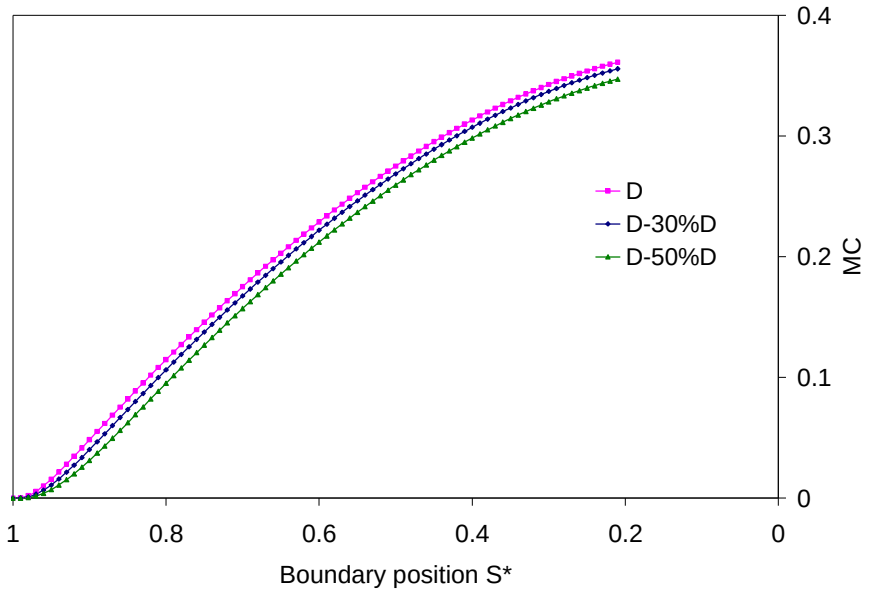

Figure 5-19: Dimensionless crystal mass deposition inside contact region, M_c, versus dimensionless moving boundary position, S^*, with different diffusion coefficients, D, as a parameter, U_S=0.05, S_o=1.1 (X=6%), $C_a = C_b = 1.0$

The sensitivity study of variation in diffusion coefficient shown in Figure 5-19 also suggests that the numerical model of recrytallization process near one contact point is applicable for a certain range of diffusion coefficients because the simulation results are not significantly changed when a 50% decrease of diffusion coefficient is used. From the values of diffusion coefficients for KCl, NaCl and $MgCl_2$ show in Table 4-1, it

implied that these simulation results are equally valid for NaCl and $MgCl_2$ and the numerical model may be applied for typical chemical solutions on potash particle surfaces consisting of KCl, NaCl and $MgCl_2$.

The sensitivity studies on other parameters used in this numerical model such as time step, space grid and tolerance are presented in Appendix D.

5.4 Conclusions and Summary

In this chapter, a theoretical/numerical model is formulated to investigate the recrystallization process near one contact point between two salt particles. To study this problem, potash fertilizer properties are used and some geometric simplifications are introduced near the contact point but the conditions simulated are typical of other tests and field conditions. The effects of three independent factors are investigated separately using this model. These are initial moisture content, X, evaporation rate or liquid film speed, U_S, and degree of supersaturation on the surrounding surface, C_b. The numerical results show that the mass of crystal deposition near the contact point will increase with increased initial moisture content and decrease with evaporation rate. These numerical predictions are consistent with the experimental data of cake strength of potash particle beds after a specified wetting and drying process. The numerical investigation of variations in the bounding solid surface degree of supersaturation near the contact point showed variations in the mass deposition per unit area near the contact point. This prediction is consistent with experimental finding of Sun who showed increased surface roughness NaCl and KCl surface after wetting and drying implying significant variations in the recrystallization surface degree of saturation during this process.

It is concluded from the numerical investigation that the recrytallization near the contact point is the prime factor to cause a caking process in a particle bed. The relationship between cake strength and initial moisture content, drying time, particle size and chemical composition can be explained by the simulation of this numerical model. It is also concluded that numerical simulation results are equally valid for a wide range of salts such as KCl, NaCl and $MgCl_{2.}$

CHAPTER 6

SUMMARY, CONCLUSIONS AND FUTURE WORK

6.1 Summary

In this study, the problems of product caking for bulk granular potash stored in vessels or storage bins are investigated using laboratory tests. The general purpose of this research is to investigate the effects of some prime factors such as initial moisture content, particle size, drying time and chemical composition on cake strength. The first key objective was to develop a new test method to accurately measure cake strength and investigate the factors that influence cake strength using this method. Then the second objective was to develop and validate a theoretical/numerical model that can simulate/predict the caking process near contact points between particles.

The following points summarize the work carried out by this research:

1. A new test facility was devised and designed which can be used to accurately measure cake strength of a caked potash bed. A centrifugal loading method has been developed to determine the area-averaged fracture tensile stress in a ring of caked potash fertilizer. A theoretical model of stress analysis in a two-dimensional plane was developed.

2. A series of tests were conducted to measure cake strength of caked potash samples in which the initial moisture content, particle size, drying time and chemical composition (i.e. content of magnesium) were varied. The effect of these factors on cake strength and its uncertainty were investigated and quantified experimentally.

3. A theoretical/numerical model was developed to simulate ion diffusion and crystallization process near one contact point between two potash (KCl) particles during a typical drying process. The moving boundary problem (i.e. one-dimensional Stefen problem) was formulated considering the moving air-liquid interface around the particle surface. A FORTRAN program was developed based on this model and specified boundary conditions.

4. The numerical model was used to investigate the effects of three independent factors such as initial moisture content, evaporation rate, and degree of supersaturation on the surface surrounding the contact point. The simulated results were compared to the experimental cake strength data and the roughness measurements and the numerical model was shown to be consistent with experimental data.

6.2 Conclusions

1. The new centrifugal method of cake strength measurement developed in this thesis can be used to measure cake strength with smaller uncertainties for a typical caked sample bed of bulk materials such as potash. Experimental correlations between cake strength and some important factors such as initial moisture content, particle size, drying time and chemical composition can be predicted using this method for various sample preparations considering these factors. It is found that cake strength

increases linearly with greater initial moisture content and a slower drying process produces a stronger cake. It is also found that cake strength decreases with increasing particle size for the same initial moisture content and drying method and cake strength will increase essentially linearly with magnesium content for samples with the same initial moisture content, particle size and drying method.

2. The developed theoretical/numerical model can be used to predict ion diffusion and recrystallization process near one contact point between two salt particles such as KCl during a typical drying process. The effects of initial moisture content, drying rate and degree of supersaturation on the surrounding surface on the recrystallization process can be investigated numerically using this model. The simulated results for the crystal mass deposition near contact points between particles are consistent with the experimental studies of cake strength and surface roughness after caking.

3. This numerical model can be used to explain the relationship between cake strength and initial moisture content, cake strength and the rate of drying, cake strength and salt impurities on the particle surfaces, and enhanced surface roughness on caked surfaces after caking compared to the roughness before wetting. Although qualitative agreement between this recrystallization theory and experimental data is evident from these findings, quantitative agreement will require the measurement of more data and the use of more complex boundary conditions in the analysis and likely more sophisticated experimental techniques and chemical analysis.

4. The theoretical modelling investigation indicates that, as hypothesized by other researchers, recrystallization from wetted particle surfaces near contact points between potash particles in beds or bulk storage is the primary cause of caking.

6.3 Hypothesis

The centrifugal method to measure cake strength for one particular bulk material, potash, are thought to be applicable for a wide range of the bulk materials which are susceptible to caking. The numerical results simulated by the theoretical/numerical model for the recrystallization process near one contact point between two particles are equally valid for a wide range of salts such as NaCl and $MgCl_2$.

6.4 Future Work

Although the current theoretical/numerical model can simulate the recrytallization process near one contact point between two potash particles which is the most likely mechanism of caking in a potash bed, it is still at elementary level for caking process in actual potash storage beds. Therefore, more experimental and theoretical/numerical work should be done to characterize caking. Recommendations for future work are as folows:

1. Future work should be done on the theoretical/numerical model of recrystallization near a contact point between two particles considering following points: 1) another moving boundary condition should be included in the numerical model considering the crystal layer growth at the liquid-solid interface; 2) the relative size of the contact region between two potash particles, r_c ,should be analyzed and calculated

and the relationship between contact region and liquid film thickness surrounding particle surfaces should be determined; 3) the model should be modified to take into account the effect of surface tension on the recrystallization process near the contact point; and 4) the evaporation rate could be influenced by the thermal changes caused by latent effects during the drying process so the model should be modified to consider the changed evaporation rate.

2. When potash is stored and transported, the ambient temperature and relative humidity often change. These changes lead to cyclic processes for salt dissolution and recrystallization in the potash beds. Experiments should be carried out to measure cake strength of caked potash sample subject to cyclic wetting and drying processes. Corresponding to the experimental investigation, the dissolution process should be included in the numerical model and the effects of cyclic wetting and drying on final cake strength should be studied numerically.

3. Zhou (2000) measured the effective thermal conductivity of a potash bed and showed that the thermal conductivity of caked potash increased 20% compared to uncaked potash. More experimental studies should be conducted to explore the relationship and the correlation between effective thermal conductivity and cake strength for a potash bed.

4. The experimental work could be expanded to cover a wide range of properties and test conditions to validate the numerical model of recrystallization near a contact point between two potash particles. As well, more sophisticated experiments would be needed to directly relate crystal bridging near contact points and the test

conditions such as initial moisture content and the evaporation rate of water from thin films surrounding particles.

REFERENCES

Arinze, E.A., S.Sokhansanj, Besant, R.W., Wood, H.C., and Schoenau, G.J., 2000 Moisture Adsorption Characteristics of Granular Potash during Storage-Caking, *ASAE Annual International Meeting*.

Arinze, E.A., S.Sokhansanj, Besant, R.W., Wood, H.C., and Schoenau, G.J., Effects of Material & Environmental Conditions on Caking & Breakage of Potash Fertilizer Products during Storage, Shipment & Handling, *Powder Handling Processing*, 2001. 13(1), 45-54.

ASME PTC 19.1 Uncertainty Analysis, 1998.

ASTM Standards, C39/C39M-03, 2003 Standard Test Method for Compressive Strength of Cylindrical Concrete Specimens, ASTM International.

ASTM Standards, D6128-00, 2000 Standard Test Method for Shear Testing of Bulk Solids Using the Jenike Shear Cell, ASTM International.

Budynas, R.G., 1999 Advanced Strength and Applied Stress Analysis, 2nd edition, Boston: WCB/McGraw-Hill.

Carslaw, H.S, Jaeger, J.C. *Conduction of Heat in Solids*, 2nd , Clarendon Press, Oxford 1959

Chen, C.K. and Tien, C.-L., Conductance of Packed Spheres in Vacuum, *ASME J. Heat Transfer,* 1973, 95, 302-308

Chen, R., Chen, H., Besant, R.W., and Evitts, R.W., Properties Required to Determine Moisture Transport by Capillarity, Gravity, and Diffusion in Potash Beds, *Ind. Eng. Chem. Res.* 2004, 43, 5365-5371.

Craig, R.R., 2000 Mechanics of Materials, 2nd edition, John Wiley &Sons. Inc.

Crank, J. *Free and Moving Boundary Problems*, Clarendon Press, Oxford 1984.

CRC handbook of Chemistry and Physics, 79th Edition, 1998-1999.

Felbeck, D.K., Atkins, A.G., 1984 Strength and Fracture of Engineering Solids, Prentice-Hall, Inc., Englewood Cliffs.

Gao, Q. Measurement and Modeling of an Air Wall Jet Over Potash Surfaces, M.*Sc Thesis*, University of Saskatchewan, 2001

Garrett, D.E., 1996 Potash Deposit, Processing, Properties, and Use, Chapman & Hall, London.

Gillies, D., Wang, Y., Evitts, R.W., Besant, R.W., Effects of Moisture Content, Particle Size and Chemical Content on the Cake Strength of Potash (accepted by The 5th International Conference for Conveying and Handling of Particulate Solids), 2006

Hu, G., Otaki, H., Lin, M., 2001 An Index of The Tensile Strength of Brittle Particles, Minerals Engineering, Vol. 14, No. 10, pp1199-1211.

Kaviany, M., 1999 Principles of Heat Transfer in Porous Media, 2nd edition, Springer-Verlag New York.

Kollmann T. H. and Tomas J, 2001 Time Consolidation and Caking Behaviours of Soluble Particulate Solids, Bulk Solids Handling 21 (4), pp. 431-434.

Leaper, M.C., Berry, R.J., Bradley, M.S.A., Bridle, I., Reed, A.R., Abou-Chakra H. and Tüzün, U., 2003 Measuring the tensile strength of caked sugar produced from humidity cycling, Proceedings of the Institution of Mechanical Engineers, Part E: Journal of Process Mechanical Engineering, v 217, n1, p41-47.

Muller-Krumbhaar, H., Diffusion Theory for Crystal Growth at Arbitrary Solute Concentration, *The Journal of Chemical Physics*, 1975, 63(12), 5131-5138.

Mullin, J. W., *Crystallization*, 3rd edition, Butterworth-Heinemann, 1993.

Newman, J., *Electrochemical System*, Prentice-Hall, Inc. Englewood Cliffs, 1973.

Peng, Shi-wen, Strathdee, Graeme and Besant, R.W., Dissolution Reaction of Potash Fertilizer with Moisture, *The Canadian Journal of Chemical Engineering*, 1999. Vol 77, pp1127-1133

Pietsch, W.B., 1969 The Strength of Agglomerates Bound by Salt Bridges, The Canadian Journal of Chemical Engineering , Vol. 47, pp403-409.

Pilkey, W. D., 2005 Formulas for Stress, Strain and Structural Materials, John Wiley& Sons, Inc.

Rumpf, H., 1958 Grundlagen und Methoden des Granulierens. Chemie Ing. Tech., 30, p144-158.

Sun, J., Besant, R.W., Evitts, R.W., Fracture Stress Measurement and Images of Caked particles of KCl and NaCl (accepted by The 5th International Conference for Conveying and Handling of Particulate Solids), 2006

Tanaka, T., 1978 Evaluating the Caking Strength of Powder, Ind. Eng. Chem. Prod. Res. Dev., Vol. 17, No. 3, pp241-246.

Thompson, D.C., Fertilizer Caking and Its Prevention, *Proceeding of Fertilizer Society*, No. 125, London, UK. 1972.

Tsypkin, G.G., Brevdo, L, A Phenomenological Model of the Increase in Solute Concentration in Ground Water Due to Evaporation, *Transport in Porous Media*, 1999, 37, 129-151.

Walker, G. M., Magee, T.R., Holland, C.R., Ahmad, M.N., Fox, J.N., Moffat, N. A. and Kells, A.G., Caking Process in Granular NPK, *Ind. Eng. Chem. Res*., 1999, 37, 435-438.

Wang, W., Hu, W.R., Concentration Distribution in Solution Crystal Growth: Effect of moving interface conditions, *Journal of Crystal Growth*, 1999, 203, 227-233.

Yao, L.S., Prusa, J., Melting and Freezing, *Advances in Heat Transfer, Volume 19*, Academic Press, INC. 1989

Yungwirth, T., Evitts, R.W., Besant, R.W., Measuring Moisture Content of Potash Bulk Fertilizers Using a Steel Ball in a Transient Heat Transfer Process, *Ind. Eng. Chem. Res.*, (accepted for publication 2006)

Zhou, Q, Measurement and Simulation of Transient Moisture and Heat Diffusion in a Potash Layer, *M.Sc Thesis*, University of Saskatchewan, 2000.

APPENDIX A

MEASUREMENT OF BOND STRENGTH BETWEEN CAKED POTASH AND PVC PLATE

A simple test has been conducted to measure the bond strength between caked potash and PVC plate using the device shown in Figure A-1.

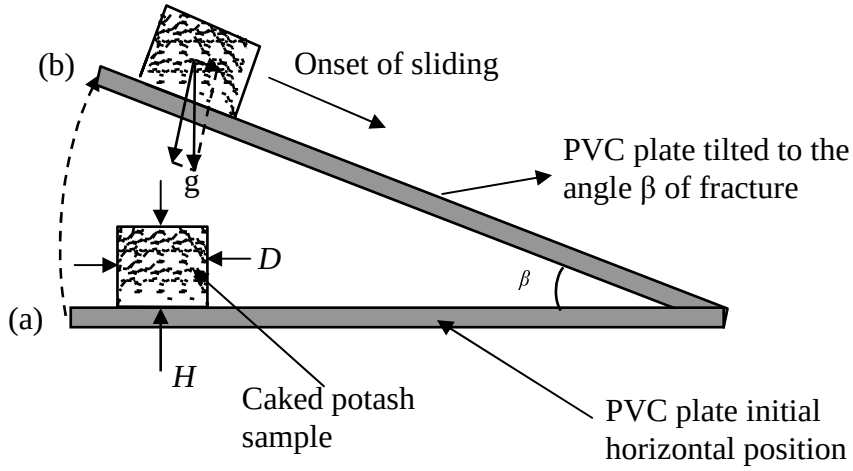

Figure A-1: Schematic of a device to measure the bond strength between PVC plate and a caked potash specimen

In this test a cylindrical wetted potash sample, 203 mm in high, *L*, and 64 mm in diameter, *D*, with 3% initial moisture content, was made onto the PVC plate. After oven drying at 40^{o}C, this sample was expected to cake onto the PVC plate. During the test, the caked potash sample on PVC plate was tilted from position (a) to position (b) as shown in Figure A-1. The average shear stress at the angle of fracture, β, between the potash sample and PVC plate is given by,

$$\tau_b = \frac{mg\sin\beta}{\pi(D/2)^2} \qquad \text{(A-1)}$$

Where, m is mass of the caked potash sample which is given by $m = \rho H \pi D^2 / 4$;

The selected particle size of potash sample is ranged from 0.85 mm to 1.18 mm. 5 samples were repeated and the experimental results for the fracture shear stress were 131.8 Pa, 115.9 Pa, 100.25 pa, 84.9 Pa and 108.2 Pa respectively which gave a mean fracture value of 108.1 Pa. Using Mohr's circle, the tensile stress at the fracture surface to break the crystal bond between caked potash and PVC plate in Figure A-1 should have the same order of magnitude as the shear stress. This bond strength between caked potash and PVC plate is much smaller than the cake strength measured for caked potash in the centrifuge under similar conditions (i.e. 40 KPa). This test implies that the radial tensile stress on the inner plastic surface of a caked potash shell shown in Figure 2-2 would be negligible compared to the inter-particle tensile stress for a ring test sample placed in the centrifuge. This experimental finding is used to determine the boundary conditions in the stress analysis model which was presented in Chapter two.

APPENDIX B

ELASTIC PROPERTY DATA FOR A CAKED POTASH SAMPLE

The literature on potash gave elastic property data for solid KCl specimens but none for caked potash particle specimens. In this experiment, Young's modulus, E_b, and Poisson's ratio, v, were determined using a compression test of a caked potash specimen. This compression test for a caked potash sample was conducted using the INSTRON material testing machine. The experimental data for a caked potash specimen shows that these mechanical properties of a caked potash bed are significantly different than those for solid KCl crystal salt specimens (i.e. 2.5×10^{10} Pa for Young's modulus and 0.3 for Poisson's ratio).

1. Experiment procedure

Potash particles with a particle size range from 0.85 mm to 1.18 mm and with 0.1% magnesium content were selected to prepare the test sample. A cylindrical caked potash sample, 200 mm in high, L, and 100 mm in diameter, D, was made by drying this specimen for 48 hours in oven at 40 ^{o}C after it was wetted with 3% moisture content. This caked sample then was placed into the INSTRON material testing machine (Model 1122) and two dial indicators were used to measure displacements in the uniaxial and lateral directions. The load cells in the INSTRON machine have a range from 0 to 5000 N. The full scale of the dial indicator used in uniaxial direction is from 0 to 25 mm with

a scale resolution of 0.01 mm. The lateral direction indicator has a full scale from 0 to 1 inch with a scale resolution of 0.001 inch (0.025 mm). Figure B-1 shows the photo of the experimental facilities and the loading test sample for compression.

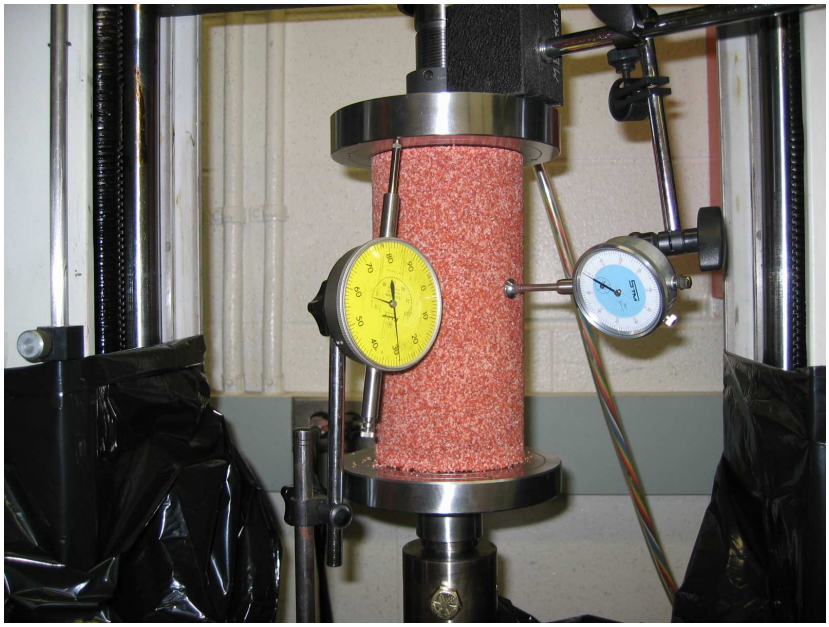

Figure B-1: Compression test in the INSTRON machine used to determine Young's modulus and Poisson's ratio for a caked potash sample

During this test, the loading speed was selected as 0.1 mm/min and the load was increased from 200 to 1000 N. The readings of the two dial indicators were recorded for each a 66.7 N increase in load above 200 N.

2. Experimental Results

Young's modulus for a specimen in compression, E_b, is defined as the ratio of stress to strain and is given by,

$$E_b = \frac{\sigma_c}{\varepsilon_a} \tag{B-1}$$

where σ_c is the stress which is given by the loading force, *F*, divided by the cross-sectional area of sample; ε_a is the strain in the uniaxial direction of loading which is given by the displacement in the axial direction, ΔL, divide by the original length. The calculation of E_b is given by equation (B-2),

$$E_b = \frac{\sigma_c}{\varepsilon_a} = \frac{4F/(\pi D^2)}{(\Delta L / L)} \tag{B-2}$$

The Poisson's Ratio in compression is defined as the ratio of the lateral strain, ε_l, to the axial strain, ε_a, which is given by,

$$\nu = \frac{\varepsilon_l}{\varepsilon_a} = \frac{\Delta D / D}{\Delta L / L} \tag{B-3}$$

The experimental data and calculated Young's modulus and Poisson's ratio are shown in Table B-1. For pure solid potassium chloride crystals, Poisson's ratio and the Young's modulus were reported to be 0.3 and 2.5×10^{10} Pa respectively (Garrett, 1996). It is found from the data in Table B-1 that the stiffness of a caked potash particle bed is significantly lower than the pure solid KCl.

Table B-1: Experimental data and uncertainty to determine Young's modulus and Poisson's ratio for a caked potash specimen comprised of particles with a size range 0.85 to 1.18 mm which is 200 mm long and 100 mm diameter

Loading (N)	$\Delta L \times 100$ (mm)	$\Delta D \times 1000$ (mm)	E_b (Pa)	$U(E_b)$ (Pa)	ν	$U(\nu)$
200.0	13.5	0	3.77×10^{7}	2.5×10^{4}	0.00	N/A
266.7	19.0	0	3.58×10^{7}	2.0×10^{4}	0.00	N/A
333.3	26.0	0	3.27×10^{7}	1.5×10^{4}	0.00	N/A
400.0	33.0	0	3.09×10^{7}	1.3×10^{4}	0.00	N/A
466.7	41.0	0	2.90×10^{7}	1.1×10^{4}	0.00	N/A
533.3	47.0	0	2.89×10^{7}	1.0×10^{4}	0.00	N/A
600.0	51.5	0	2.97×10^{7}	1.0×10^{4}	0.00	N/A
666.7	56.0	0	3.03×10^{7}	1.0×10^{4}	0.00	N/A
733.3	62.0	4	3.01×10^{7}	0.9×10^{4}	0.01	0.05
800.0	69.0	20	2.95×10^{7}	0.9×10^{4}	0.06	0.04
866.7	73.0	30	3.02×10^{7}	0.8×10^{4}	0.08	0.04
933.3	78.0	46	3.05×10^{7}	0.8×10^{4}	0.12	0.04
1000.0	82.5	46	3.09×10^{7}	0.8×10^{4}	0.11	0.03

APPENDIX C

MEASURED DATA FOR CAKE STRENGTH

Table C- 1: Average (15 samples) cake strength for different particle diameters and initial moisture contents for oven drying at 40º C

Particle size (mm)	Initial moisture content, %(w/w)	σ_{mean} (KPa)	$U(\sigma_{mean})$ (KPa)
$0.85 < d_p < 1.18$ $d_{pm} = 1.02$	0.44	0.9	0.2
	0.86	7.2	1.2
	1.76	29.5	2.9
	2.72	39.1	3.5
	3.68	56.7	2.7
$1.18 < d_p < 1.68$ $d_{pm} = 1.43$	0.92	5.9	1.8
	1.83	17.7	2.6
	2.72	20.1	1.9
$2.00 < d_p < 2.36$ $d_{pm} = 2.18$	0.90	0.80	0.4
	1.86	4.1	1.4
	2.68	10.3	2.5
$2.80 < d_p < 3.35$ $d_{pm} = 3.08$	0.88	0.5	0.1
	1.39	0.8	0.3
	1.78	1.5	0.5
	2.68	4.7	0.7

Table C- 2: Average (15 samples) cake strength at different particle diameters and initial moisture contents for air drying

Particle size (mm)	Initial moisture content, %(w/w)	σ_{mean} (KPa)	$U(\sigma_{mean})$ (KPa)
$0.85 < d_p < 1.18$ $d_{pm} = 1.02$	0.84	1.8	0.3
	1.27	2.9	0.5
	1.75	4.8	0.8
	2.70	11.9	1.3
	3.37	15.9	1.7
	5.75	31.0	2.1
	0.84	1.8	0.3
$1.18 < d_p < 1.68$ $d_{pm} = 1.43$	0.89	2.5	0.5
	1.82	3.9	0.6
	2.74	8.1	1.0
$2.00 < d_p < 2.36$ $d_{pm} = 2.18$	0.87	1.7	0.4
	1.74	2.1	0.5
	2.59	2.9	0.6
$2.80 < d_p < 3.35$ $d_{pm} = 3.08$	1.32	0.8	0.1
	1.74	1.1	0.3
	2.65	2.3	0.4

Table C- 3: Average (15 samples) cake strength at different magnesium concentrations and initial moisture contents for oven drying at 40º C, $0.85 < d_p < 1.18$ mm

Magnesium Concentration (%)	Initial moisture content, %(w/w)	σ_{mean} (KPa)	$U(\sigma_{mean})$ (KPa)
0.02	0.51	2.0	0.7
	0.93	7.3	1.5
	1.83	25.9	4.2
0.06	0.52	8.1	1.4
	0.94	15.2	1.5
	1.84	39.8	3.7
0.10	0.51	12.7	1.7
	0.92	24.4	4.3
	1.83	47.2	5.1

Table C- 4: Average (15 samples) cake strength at different magnesium concentrations and initial moisture contents for air drying, $0.85 < d_p < 1.18$ mm

Magnesium Concentration (%)	Initial moisture content, %(w/w)	σ_{mean} (KPa)	$U(\sigma_{mean})$ (KPa)
0.02	0.88	4.2	0.6
	1.84	9.0	1.1
	2.81	12.8	2.4
0.06	0.87	9.5	2.1
	1.82	19.3	2.0
	2.68	32.5	2.3
0.10	0.93	22.8	5.4
	1.85	55.7	6.9
	2.76	69.3	8.1

APPENDIX D

SENSITIVITY STUDY ON PARAMETERS USED IN NUMERICAL MODEL

The sensitivity of parameters used in this numerical model such as time step, space step in *Z* direction and criteria of convergence (i.e. tolerance) was studied. The simulation results with different time steps, space steps in Z direction and tolerances are shown in Figure D-1, D-2 and D-3 respectively.

1. Time Step (Δt)

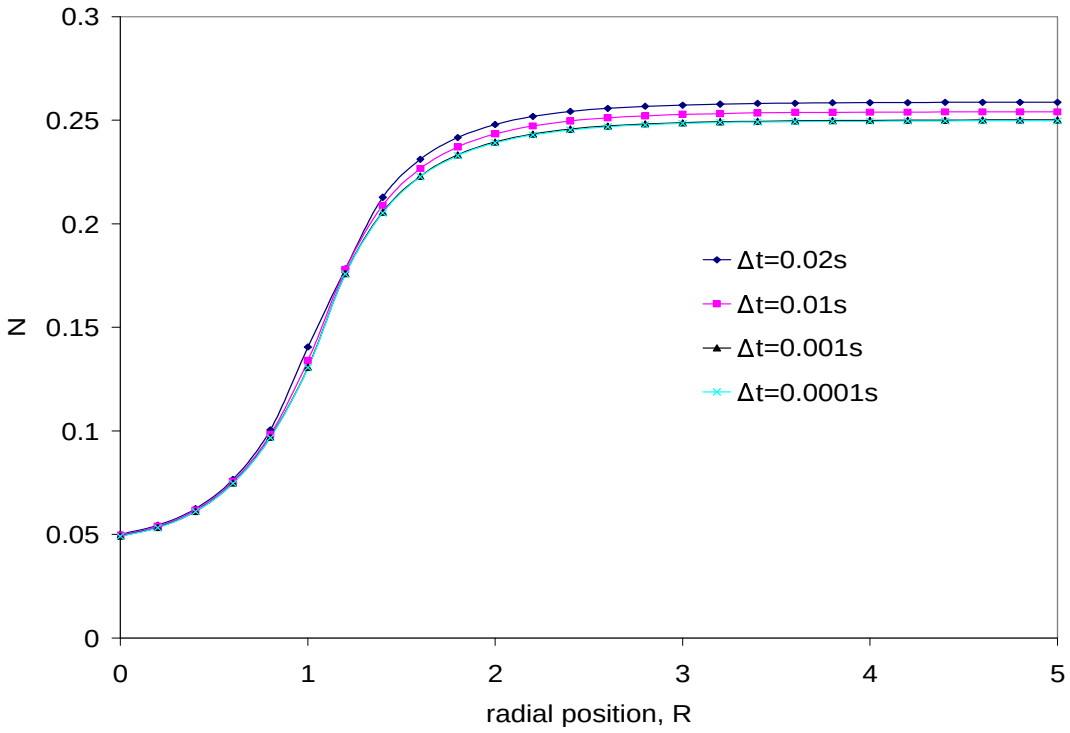

Figure D-1: Crystal mass deposition per unit area, *N*, at various radial position, *R*, with different time step, Δt , as a parameter, S_o=1.1, U_S=0.05， S*=0.2, $\Delta Z = 1/25$

2. Space step in *Z* direction (*ΔZ*)

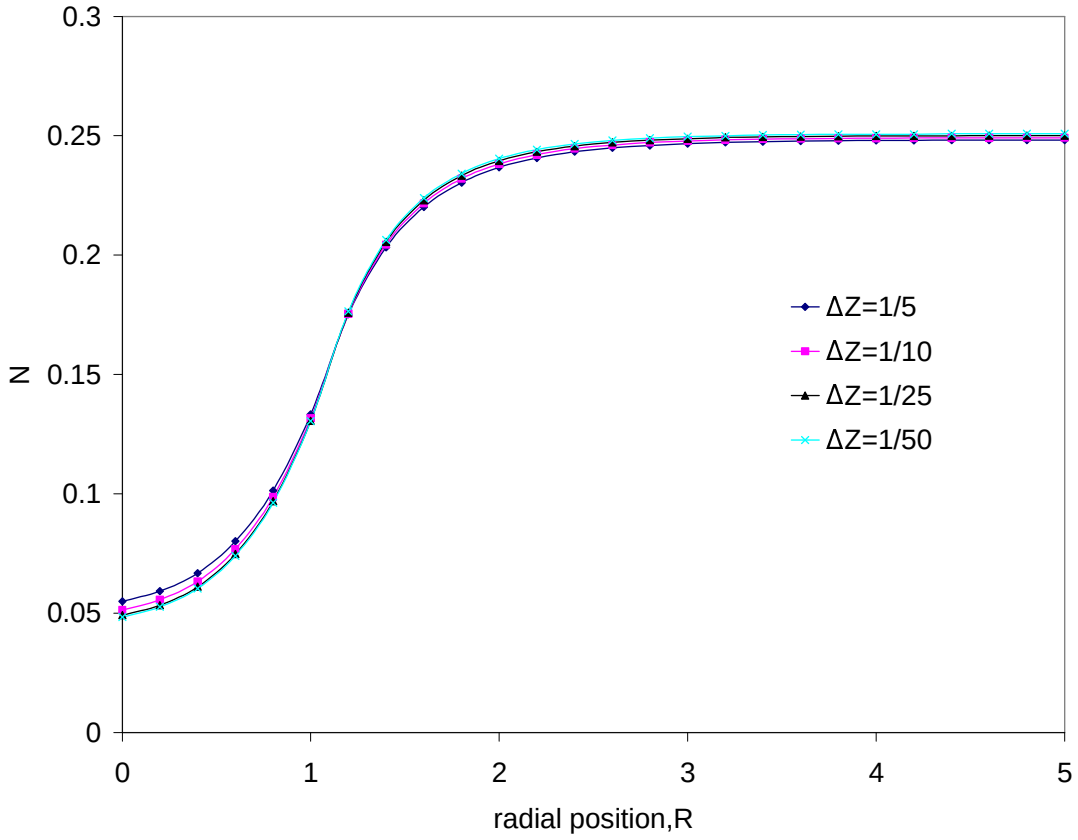

Figure D-2: Crystal mass deposition per unit area, *N*, at various radial position, *R*, with different space step, ΔZ , as a parameter, S_o=1.1, U_S=0.05， S*=0.2, $\Delta t = 10^{-3}\,s$

3. Tolerance (ε)

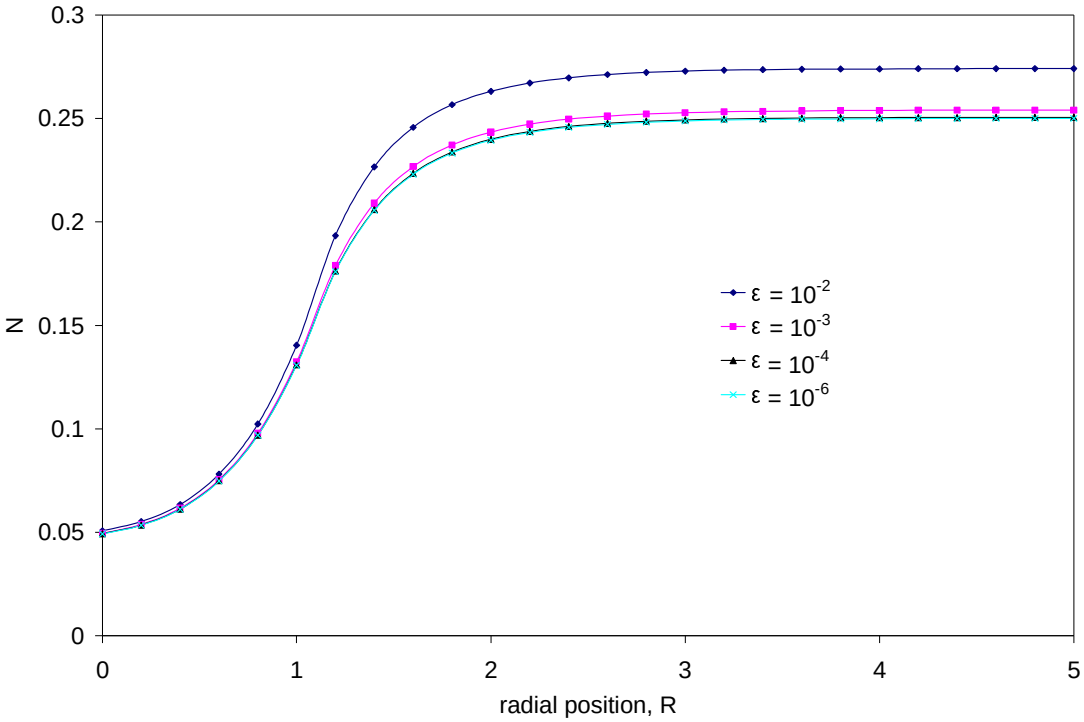

Figure D-3: Crystal mass deposition per unit area, N, at various radial position, R, with different tolerance, ε, as a parameter, S_o=1.1, U_S=0.05, S^*=0.2, $\Delta t = 10^{-3}\,s$, $\Delta Z = 1/25$